

$^{58}\text{Ni} + n$ transmission, differential elastic scattering, and capture measurements and analysis up to 813 keV

C. M. Perey, F. G. Perey, J. A. Harvey, N. W. Hill, N. M. Larson, R. L. Macklin, and D. C. Larson
Oak Ridge National Laboratory, P.O. Box 2008, Oak Ridge, Tennessee 37831

(Received 8 June 1992)

High-resolution neutron cross section measurements for ^{58}Ni -enriched targets were made at the Oak Ridge Electron Linear Accelerator of transmission below 20 MeV, of differential elastic scattering from 10 keV to 5 MeV, and of capture from 2.6 keV to 2.5 MeV. The transmission data were analyzed from 0.1 to 813 keV with a multilevel R -matrix code which uses Bayes' theorem for the fitting process. This code provides energies and neutron widths of resonances within the analyzed region, as well as a possible parametrization for resonances external to that region, as a way of describing the smooth cross section over the entire energy range. The differential elastic data at different scattering angles were compared to theoretical calculations from 30 to 813 keV using an R -function code which is based on the Blatt-Biedenharn formalism. Various combinations of spin and parity were tested to predict cross sections for the well-defined $l > 0$ resonances, and comparison with the data then provided spin and parity assignments for most of these resonances. The capture data were analyzed from 5 to 450 keV with a least-squares fitting code using the Breit-Wigner formula. The resulting set of resonance parameters yields values for the thermal total and capture cross sections within experimental uncertainties. A total of 482 resonances are reported, of which five are fictitious s -wave resonances outside the analyzed energy region and 61 are seen and analyzed only in the capture data. The reduced widths of the 61 s -wave resonances follow the Porter-Thomas distribution and their nearest neighbor spacings agree with the Wigner distribution. The average s -wave level spacing is 13.1 ± 0.9 keV and the s -wave strength function is $(3.2 \pm 0.6) \times 10^{-4}$. Since most of the large non- s -wave resonances have their angular momentum assigned with confidence, the strength functions for the p - and d -wave resonances could be determined; values are $(1.3 \pm 0.2) \times 10^{-4}$ and $(3.0 \pm 0.4) \times 10^{-4}$, respectively. The level densities calculated with the Fermi-gas model for $l = 0$ and $l > 0$ resonances are compared with the cumulative number of observed resonances. The average radiation widths were deduced from resonances analyzed in the three data sets below 450 keV. The mean values and standard deviations of the distributions of the radiation widths are 2.3 ± 1.7 eV for the s -wave resonances, 0.77 ± 0.32 eV for the p -wave resonances, and 1.4 ± 0.5 eV for the d -wave resonances. The average capture cross section as a function of the incident neutron energy is compared to a prediction based on the tail of the giant electric dipole resonance.

PACS number(s): 25.40.Dn, 25.40.Lw, 25.40.-h

I. INTRODUCTION

The neutron cross sections of structural materials in the iron region are important in reactor applications because of the stainless steels that are used. As part of a program to provide state-of-the-art resonance parameters for nuclei in this mass region, high-resolution neutron transmission, capture, and scattering measurements from ^{58}Ni were performed at the Oak Ridge Electron Linear Accelerator (ORELA). Resonance parameters resulting from the concurrent analysis of those measurements are reported here; these parameters supersede results published earlier [1,2] which were based on partial data.

Preliminary results from analysis of the same data used here have been published in an Oak Ridge National Laboratory report [3]; the resonance parameters given in the ENDF/B-VI evaluation [4] for this nucleus are essentially those of Ref. [3], with modifications to agree with data at thermal energy. Results reported here represent a slight improvement over results from Ref. [4].

As found in the analysis of other ORELA transmission data in this mass region [5], in order to obtain a good fit

to the data above ≈ 200 keV using a single set of parameters it was necessary to use a different channel radius for the p -wave channel from that used for the s - and d -wave channels. The set of resonance parameters reported in this paper describes the total cross section satisfactorily from thermal to energies slightly above 800 keV. From the analysis of the differential elastic-scattering data, the angular momentum of approximately 75% of the non- s -wave resonances seen in the transmission data can be determined with confidence.

Our results are compared with earlier results obtained from analyses of transmission [6,7] and capture data [8,9] taken at other establishments. From these comparisons we conclude that a concurrent analysis of the three data types provides a great deal more information than their independent analyses, that we are able to obtain good fits to the data up to higher energies, and that in a given energy region we can analyze a greater number of narrow resonances.

The discussion of our results and of the extraction of the average parameters is also valid for the resonance parameters used in ENDF/B-VI [4].

II. DATA ACQUISITION AND DATA PROCESSING

The transmission, capture, and differential elastic-scattering measurements were made by the time-of-flight technique using neutron pulses from the ORELA water-moderated tantalum target. Collimators were utilized to focus primarily on moderated or unmoderated neutrons from the target, depending on the measurement. Table I gives the main characteristics for each measurement.

A. Transmission measurements

Two measurements were made with a 78.217 ± 0.004 -m flight-path length with two different neutron detectors using only water-moderated neutrons. The transmission measurement with a 201.578 ± 0.005 -m flight-path length used mainly unmoderated neutrons produced in the tantalum target.

The measurements with moderated neutrons using the 78-m flight path were made on two samples weighing 49.98 and 4.997 g with thicknesses of 0.0764 and 0.007 70 atom/b of nickel enriched to 99.93% in ^{58}Ni . Data taken with the thin sample were not analyzed. For the energy region from 100 eV to 200 keV, the detector was a 1.3-cm-thick, 11-cm-diam ^6Li -glass scintillator mounted on a RCA 4522 photomultiplier tube. The electron beam burst was 40 ns wide, producing a beam power on the target of 50 kW at 800 Hz. Two filters were inserted in the beam at 5 m: a 1-g/cm^2 ^{10}B filter to eliminate low-energy neutrons due to preceding bursts and a 0.6-cm-thick lead filter to reduce the gamma-flash intensity. Transmission data from 4 to 1500 keV were obtained using a 2.5-cm-thick, 7.5-cm-diam NE-110 proton recoil scintillator, also mounted on a RCA 4522 photomultiplier. The electron beam burst was 4 ns wide, producing a beam power of 8 kW at 1000 Hz. Two filters were again inserted in the neutron beam at 5 m: a 1-g/cm^2 ^{10}B filter and a 0.7-cm-thick ^{328}U filter. For this second measurement, the detectors were gated off during the gamma flash and the succeeding $\approx 5 \mu\text{s}$ to eliminate possible extraneous events due to phototube afterpulsing.

The 200-m transmission measurement was made with an "effective" sample enrichment of 99.99% ^{58}Ni , achieved by the use of a 0.005-cm-thick foil of natural

nickel in the open beam to compensate for the ^{60}Ni in the 52.40 g of nickel enriched to 99.93% in ^{58}Ni ; the sample thickness was 0.1724 atom/b. A 2.5-cm-thick, $5.2 \times 8.9\text{-cm}^2$ NE-110 scintillator mounted between two RCA 8854 photomultipliers was used as the neutron detector. The neutron beam was collimated to pass only through the scintillator. The electron beam burst was 5 ns wide, producing a beam power of 6 kW at 800 Hz. The measurements covered the neutron energy region from 100 keV to 20 MeV. The energy resolution was determined mainly by the electron beam burst width; the full width at half maximum (FWHM) of the resolution function, in percent, is approximately $0.07[E(\text{MeV})]^{1/2}$. Two filters were inserted in the beam at 5 m: a 0.3-g/cm^2 ^{10}B filter to reduce overlap neutrons and 4.4 cm of uranium to reduce the intensity of gamma flash from the tantalum target. Data were acquired using an EG&G time digitizer and were corrected first for the dead time (1104 ns) of the digitizer, then for the backgrounds.

For the 78-m transmission data taken with the ^6Li -glass detector, the maximum dead-time corrections were 15% with the open beam, 10% with the thick (0.0764 atom/b) sample in, and 14% with the thin (0.007 70 atom/b) sample in. With the NE-110 detector, these corrections were 23% with the open beam, 18% with the thick sample in, and 22% with the thin sample in. For the 200-m data, the maximum dead-time corrections were 10% with the open beam and 6% with the sample in.

During the transmission measurements using water-moderated neutrons, three sources of backgrounds were monitored: (1) a background arising from 2.2-MeV gamma rays produced by neutron capture in the water moderator of the target, (2) a time- and beam-independent room background, and (3) a background produced from neutrons scattered by the detector. With the NE-110 detector, the third type of background arises mainly from a 478-keV gamma ray from the $^{10}\text{B}(n, \alpha\gamma)$ reaction produced from the absorption of scattered neutrons by the boron in the Pyrex face of the photomultiplier. For the 78-m transmission data taken with the ^6Li -glass detector, the background corrections for all sources were less than 3% of the open beam counting

TABLE I. Experimental conditions for data used in this analysis.

Energy range (keV)	Flight path ^a (m)	Burst width (ns)	Average sample thickness ^a (atom/b)	Detector
Analyzed transmission data				
0.1–53	78.217(4)	40	0.0764(4)	^6Li glass
53–180	78.217(4)	4	0.0764(4)	NE-110
180–813	201.578(5)	5	0.1724(4)	NE-110
Analyzed differential elastic-scattering data				
30–813	200.192(4)	8	0.033(1)	NE-110
Analyzed capture data				
5–22	40.122(4)	4	0.003 83(2)	C_6F_6
22–450	40.122(4)	4	0.0382(2)	C_6F_6

^aThe uncertainty on the last significant digits is given in parentheses.

rate. To aid in the determination of these backgrounds and to optimize the signal-to-background ratio for the NE-110 detector, four separate pulse-height spectra were recorded. The contribution of all of these backgrounds was less than 1% of the open beam over the energy region where the data were analyzed. The 200-m transmission data were corrected only for a constant background (determined at long times), since there was little neutron capture in the narrow water-cooling channels of the tantalum target and little background from 478-keV gamma rays with this detector whose two photomultipliers were out of the beam. This constant background is less than 0.3% above 180 keV.

B. Capture measurements

Pulsed ORELA-moderated neutrons passed through copper collimators to the capture cross-section apparatus 40.12 m from the neutron-producing target. A diagram with isometric sketches of significant subsections has been published [10]. The neutron flux was monitored by a thin, 0.5-mm, ^6Li -glass scintillator 447 mm ahead of the sample [11]. Neutrons with energies below about 10 eV were removed from the collimated neutron beam by a ^{10}B filter.

Thin and thick 99.935% enriched ^{58}Ni metal samples were used for the capture measurements. The sample size was 25.4 mm by 50.8 mm, nearly filling the collimated beam cross section. The samples, with thicknesses of 0.0038 and 0.0382 atom/b, were hung in thin Mylar bags between two fluorocarbon liquid scintillator cells for prompt gamma-ray detection [12]. They faced and were fully illuminated by the ORELA pulsed neutron beam.

Pulse heights from the scintillators were measured as a function of neutron time of flight in a 56 320-ns time range, corresponding to energies from 2.6 keV to 2.5 MeV. A pulse height bias of 153 keV was used. Detector efficiencies were calibrated by the saturated resonance method using the strong 4.9-eV resonance in ^{197}Au [13] and monitored for stability with long-lived packaged radiation sources before, between, and after the enriched ^{58}Ni neutron capture measurements.

The primary two-dimensional time-of-flight and prompt gamma-ray energy yield data were further processed [12] by correcting for electronic dead-time losses, which increased as a function of time of flight to maxima of 5.1% for the thin sample and 9.0% for the faster-counting quick sample. The scintillator background due to cosmic rays, uranium, thorium, and potassium in the local environment was about 48 counts/s. Accelerator-induced radioactivities with half-lives longer than microseconds increased this background rate to 69 counts/s for the thin sample and 79 counts/s for the thick one as recorded during each measurement by a 65 536-ns time gate immediately preceding each burst of neutrons. For comparison, the average detector count rate during the 56 320-ns time-of-flight data gate was 313 counts/s for the thin sample and 1461 counts/s for the thick sample.

Backgrounds induced by beam neutrons at short times were determined by auxiliary measurements. With the beam in vacuum at the sample position, the background

component due to collimator and lithium glass scattering decreased with time after the neutron pulse, but was proportional to the fast neutron intensity; therefore, this background could be scaled to the monitor count for each experiment. Expressed in units of the ^{58}Ni capture cross section, it decreased from 25 mb near 10 keV to 2.5 mb near 1000 keV for the thin Ni sample and from 3 to 0.3 mb for the thick Ni sample over the same energy range. Another background component was due to neutrons scattered by the sample itself into the detector and housing. A ^{208}Pb sample was used to evaluate this background since it gives little energy loss on scattering a neutron and has few resonances. The background component measured with the ^{208}Pb sample could be scaled both to monitor counts and to the scattering probability for the capture sample, and also shifted and broadened in energy to match the elastic-scattering versus angle relations appropriate to the atomic mass of the sample. Expressed again in units of the ^{58}Ni cross section, this background component ranged from 9 to 1.2 mb for the thin Ni sample and from 8.4 to 1.1 mb for the thick Ni sample in the energy range where these data were analyzed.

Gamma-ray energy loss in the sample was calculated to be 1.9% for the thin Ni sample and 8.9% for the thick Ni sample by a numerical integration code which includes the sample and detector geometry explicitly. This code was extensively checked against a Monte Carlo code in France [14]. Both of these calculations were based on the prompt gamma-ray spectrum produced by thermal neutron capture. For particular resonances there may be harder spectra dominated by gamma rays from 6 to 9 MeV for which the energy-loss corrections would be smaller. Some electrons above ≈ 4 MeV generated from higher-energy gamma rays in the nickel samples could penetrate to the detector liquid.

Known sources of uncertainty in the experimental work have been estimated as $\approx 4\%$ at the 68% probability level. While the gold-saturated resonance calibration has been compared to other elements with softer capture gamma-ray spectra such as holmium, silver, and uranium and agrees to about 1%, discrepancies of the order of 16% are observed for the 1.15-keV resonance of ^{56}Fe , which has a very hard spectrum [15]. Later investigations [16–19] have revealed that this discrepancy is due to an incorrect weighting function for high-energy gamma rays. We do not have sufficient information on the spectra of the resonances of ^{58}Ni to perform a correction to the capture data due to the use of an incorrect weighting function. It is, however, likely that the capture data for some of the resonances are systematically too high, possibly by as much as 16%. Correlated uncertainties associated with flux-monitor calibration above 40 keV increase slowly with energy to 3.5% at 1400 keV [20]. A 153-keV pulse-height bias was adequate for all the ^{58}Ni capture cross-section data as the threshold for the first inelastic gamma ray is 1480 keV.

C. Differential elastic-scattering measurements

The scattering measurement was done at the 200-m flight-path station. A collimator allowed both unmo-

derated and moderated neutrons to reach the sample.

The sample was made of 52.45 g of Ni powder, enriched to 99.93% in ^{58}Ni , contained in a 5.14-g hollow cylinder (5.85 cm high, 3.30 cm outside diameter, and 2.30 cm inside diameter). The cylinder was made from 0.005-cm-thick natural nickel foil, resulting in an effective enrichment of 97.0% in ^{58}Ni . The cylinder was suspended at the center of a 183-cm-diam scattering chamber, which was evacuated and isolated from the flight-path beam tube by means of a 0.025-cm Mylar entrance window.

The scattering data were obtained with a 0.3-g/cm^2 ^{10}B filter to eliminate low-energy neutrons associated with the previous burst and with two filters of ^{238}U to reduce the intensity of the gamma flash from the target. One ^{238}U filter (0.5 cm thick) covered the whole collimator; the other (2.5 cm thick) shadowed only the tantalum part of the target. The measurements covered the energy region from approximately 10 keV to 5 MeV. The electron beam burst width was 8 ns resulting in an energy resolution (FWHM) at higher energies of approximately $0.11[E(\text{MeV})]^{1/2}\%$.

Six neutron detectors were located 19.1 cm from the center of the chamber at angles of 39° , 55° , 90° , 120° , 140° , and 160° from the direction of the incident neutron beam. Each neutron detector consisted of a 7.62-cm-long by 4.32-cm-diam cylinder of NE-110, which was viewed at each end by RCA 8850 photomultiplier tubes. Additional details of the experimental arrangement for these scattering measurements can be found in Ref. [21]; information on the calculated efficiencies for the two-phototube detectors is given in Ref. [22]. Data were corrected for dead time, which was caused predominantly by detection of the gamma flash scattered by the sample.

Data were also taken with one of the detectors placed in the direct beam to measure the product of the flux and the detector efficiency as a function of neutron energy.

All spectra were normalized by means of a neutron monitor detector. After correcting for dead time and constant room background, the scattering spectra were divided by the spectrum from the in-beam detector to remove effects of the energy dependence of the incident flux and detector efficiency. The data were not corrected for multiple scattering in the sample, but were corrected for geometrical factors to deduce a relative differential scattering cross section with an uncertainty of $\approx 5\%$.

III. DATA ANALYSIS

The transmission, capture, and differential elastic-scattering were analyzed interactively to generate the single set of resonance parameters given in Table II.

The absolute energy scale adopted in this analysis is the energy scale of the transmission measurements at the 200-m flight-path station. This choice is justified by accurate laser measurements of the ORELA flight-path lengths done in 1984 [23]. The uncertainties of the effective flight path lengths versus energy are discussed in detail in Ref. [24].

A. Transmission data analysis

The transmission data were analyzed with the multilevel *R*-matrix Reich-Moore [25] formalism code SAMMY [26]. SAMMY is a constrained least-squares code which uses Bayes's theorem for the fitting process. By using Bayes's equations, various data sets can be analyzed sequentially to yield a result equivalent to the simultaneous analysis of these data sets. In this work the code SAMMY was used to analyze only the transmission data, since SAMMY did not yet include corrections for multiple scattering in analysis of capture data.

Three data sets were analyzed between 0.1 and 813 keV (see Table I). From 0.1 to 180 keV, the transmission data analyzed were those obtained with the 78-m flight-path length. Below 53 keV, data from the ^6Li -glass detector were used and data from the NE-110 detector above 53 keV. Between 180 and 813 keV, the measurements taken with the 200-m flight path were analyzed.

Present in the ^{58}Ni sample is a small ^{60}Ni impurity ($\approx 0.06\%$) which contributes slightly to the smooth cross section of our data. Therefore parameter values recommended for the large *s*-wave resonances for this isotope in a recent analysis of new ^{60}Ni transmission measurements [27] were included in our analysis up to 180 keV.

In this analysis the 78-m transmission data were corrected for 1.2% water contamination of the sample and the 200-m data for 0.42% water contamination. This contamination was undiscovered prior to our earlier analysis of the data [3,4]; therefore, the fit below 14 keV was clearly unsatisfactory. The fit now obtained is shown in Fig. 1 from 0.1 to 20 keV with the 12.5–14-keV region enlarged and shown in Fig. 2 with the simultaneous fit to the capture data in the same energy region. In Fig. 1 the averaged data with their uncertainties are shown and are barely distinguishable from the theoretical curve.

A Gaussian resolution function was used in the transmission data analysis with the code SAMMY. This Gaussian resolution is a function of the electron burst width Δt and of the spread of the flight-path length distribution ΔL . The electron burst widths (approximately square functions in time) were adjusted by the code and were found to be close to the nominal values given in Table I. An exponential tail was added to the Gaussian resolution below 180 keV to account for the water moderator, which was used as neutron source in this region.

In an earlier analysis of a different element (^{56}Fe) in this mass region [5], ΔL was found to be energy dependent. This was confirmed by Monte Carlo calculations of the flight-path length distribution for the ORELA tantalum target, which showed that ΔL decreases linearly with energy in the range from 100 keV to 1 MeV [28]. Because of the relatively small energy range of the 78-m data analysis, ΔL could be kept constant at 20 mm for the ^6Li -glass detector and at 40 mm for the NE-110 detector. However, in the analysis of the 200-m data, ΔL , in meters, is given by $-3.8 \times 10^{-8}E(\text{eV}) + 0.051$.

When the transmission analysis was extended above 200 keV, a single-channel radius was inadequate to describe the transmission data. However, the transmission

TABLE II. Resonance parameters for $^{58}\text{Ni}+n$ from 100 eV to 813 keV. The transmission data analysis was performed with the following two-channel radii: $R1=6.29\pm0.01$ fm for the $l=0$ and 2 resonances and $R2=4.23\pm0.01$ fm for the $l=1$ resonances. An asterisk denotes that parameters E_0 and Γ_n for this resonance were adjusted during the final fit to the transmission data with the code SAMMY. The covariance matrix associated with these adjusted parameters is available from the authors. Note 1: Fictitious s -wave resonance outside the range of the analysis. Note 2: Resonance seen in capture data only. The value of the neutron width Γ_n was chosen to be consistent with the transmission data. When possible, the radiation width Γ_γ was set equal to the average values of 0.77 and 1.4 eV for the $l=1$ and 2 resonances, respectively. Note 3: The capture kernel and the radiation width were corrected for the neutron sensitivity of the detector. The uncertainties given for these parameters include the large uncertainties due to this correction which are combined with the statistical uncertainties.

	E_0 (keV)	Γ_n (eV)	$g\Gamma_n\Gamma_\gamma/\Gamma$ (eV)	Γ_γ (eV)	l^a	J^a	Notes
*1	-83.9	$(46.1\pm0.3)\times 10^3$		4.0	0	0.5	1
*2	-11.30	$(4.05\pm0.08)\times 10^3$		3.1	0	0.5	1
3	6.906	0.025	0.024 ± 0.001	0.77	(1)	(0.5)	2
4	12.642	0.031	0.030 ± 0.002	0.77	(1)	(0.5)	2
*5	13.318	7.28 ± 0.05	0.72 ± 0.01	0.80 ± 0.01	(1)	(0.5)	
*6	13.638	1.06 ± 0.03	0.68 ± 0.01	0.50 ± 0.01	(1)	(1.5)	
*7	15.307	1330 ± 3	0.97 ± 0.30	0.97 ± 0.30	0	0.5	3
8	17.232	0.031	0.030 ± 0.004	0.77	(1)	(0.5)	2
9	19.010	0.086	0.077 ± 0.004	0.77	(1)	(0.5)	2
*10	20.024	1.80 ± 0.14	0.29 ± 0.01	0.35 ± 0.02	(1)	(0.5)	
*11	21.145	2.48 ± 0.13	0.76 ± 0.01	0.45 ± 0.08	(1)	(1.5)	
12	24.762	0.018	0.018 ± 0.001	0.77	(1)	(0.5)	2
13	26.069	0.23	0.35 ± 0.01	0.77	(1)	(1.5)	2
*14	26.643	1.81 ± 0.12	0.96 ± 0.01	0.65 ± 0.02	(1)	(1.5)	
15	27.63	0.038	0.036 ± 0.003	0.77	(1)	(0.5)	2
16	32.261	0.29 ± 0.09	0.46 ± 0.01	1.1 ± 0.9	(1)	(1.5)	
*17	32.398	18.53 ± 0.30	1.48 ± 0.02	1.61 ± 0.02	1	0.5	
*18	34.242	1.04 ± 0.11	0.77 ± 0.01	0.61 ± 0.04	1	(1.5)	
19	35.07	0.021	0.02	0.77	(1)	(0.5)	2
*20	36.136	18.25 ± 0.28	1.57 ± 0.02	1.72 ± 0.02	0	0.5	
*21	39.553	0.90 ± 0.12	0.78 ± 0.01	0.69 ± 0.07	(1)	(1.5)	
22	44.02	0.17	0.14 ± 0.01	0.77	(1)	(0.5)	2
*23	47.908	5.69 ± 0.32	1.38 ± 0.02	0.79 ± 0.01	1	1.5	
*24	51.912	0.46 ± 0.09	0.95 ± 0.01	1.0 ± 0.4	(2)	(2.5)	
*25	52.225	1.42 ± 0.20	1.10 ± 0.01	0.90 ± 0.08	2	(1.5)	
26	54.790	0.47	0.29 ± 0.01	0.77	(1)	(0.5)	2
*27	58.705	1.27 ± 0.15	0.71 ± 0.02	0.49 ± 0.03	(1)	(1.5)	
*28	60.151	16.02 ± 0.37	0.86 ± 0.02	0.44 ± 0.01	1	1.5	
*29	61.793	17.4 ± 0.8	1.68 ± 0.03	1.86 ± 0.04	1	0.5	
*30	63.337	3798 ± 7	3.5 ± 0.7	3.5 ± 0.7	0	0.5	3
31	66.473	0.66	0.71 ± 0.02	0.77	(1)	(1.5)	2
32	68.67	0.44	0.28 ± 0.02	0.77	(1)	(0.5)	2
*33	69.917	8.1 ± 0.8	0.62 ± 0.02	0.67 ± 0.02	1	(0.5)	
34	78.09	0.37	0.25 ± 0.14	0.77	(1)	(0.5)	2
35	81.326	0.55 ± 0.17	1.29 ± 0.03	2.0 ± 1.4	(2)	(2.5)	
*36	82.881	43.7 ± 0.7	2.66 ± 0.04	1.37 ± 0.02	1	1.5	
37	83.391	4.0 ± 1.2	0.90 ± 0.02	1.16 ± 0.11	0	0.5	
*38	83.852	34.7 ± 1.3	0.25	0.25	1	0.5	
*39	83.918	2.3 ± 0.4	1.39 ± 0.02	1.00 ± 0.08	(2)	(1.5)	
40	84.88	0.27	0.20 ± 0.01	0.77	(1)	(0.5)	2
*41	89.990	10.8 ± 0.8	0.75 ± 0.01	0.81 ± 0.01	1	(0.5)	
42	92.73	0.37	0.25 ± 0.01	0.77	(1)	(0.5)	2
43	95.687	0.65	1.47 ± 0.03	2.00	(2)	(2.5)	2
44	96.98	0.55	0.64 ± 0.02	0.77	(1)	(1.5)	2
*45	97.606	21.0 ± 0.9	0.43 ± 0.02	0.44 ± 0.02	1	0.5	
*46	101.415	4.12 ± 0.30	1.28 ± 0.03	0.48 ± 0.01	2	(2.5)	
*47	105.446	11.3 ± 0.5	2.49 ± 0.03	1.40 ± 0.02	(2)	(1.5)	
48	107.12	1.0 ± 0.3	0.31 ± 0.03	0.45 ± 0.09	(1)	(0.5)	
*49	107.77	4.4 ± 0.4	1.72 ± 0.04	1.07 ± 0.04	2	(1.5)	

TABLE II. (Continued).

	E_0 (keV)	Γ_n (eV)	$g\Gamma_n\Gamma_\gamma/\Gamma$ (eV)	Γ_γ (eV)	l^a	J^a	Notes
*50	108.360	1087±4	4.8±0.3	4.8±0.3	0	0.5	3
*51	110.75	4.6±0.5	0.96±0.04	0.54±0.03	(1)	(1.5)	
52	111.49	1.6±0.5	0.85±0.04	0.58±0.08	(1)	(1.5)	
53	116.82	0.19	0.15±0.02	0.77	(1)	(0.5)	2
*54	117.883	8.9±0.6	1.15±0.04	0.62±0.02	1	1.5	
*55	119.81	3.25±0.32	2.94±0.04	1.41±0.07	2	(2.5)	
56	121.08	0.47	0.29±0.03	0.77	(1)	(0.5)	2
*57	121.426	9.0±0.6	1.71±0.04	0.95±0.03	2	(1.5)	
*58	124.020	459.3±2.8	1.56±0.15	1.56±0.15	0	0.5	3
*59	124.06	9.3±1.1	1.31±0.05	0.70±0.03	(1)	(1.5)	
*60	125.32	2.10±0.29	2.64±0.04	1.51±0.16	2	(2.5)	
*61	129.970	13.2±1.1	0.78±0.02	0.40±0.01	1	1.5	
62	132.83	0.81	0.79±0.02	0.77	(1)	(1.5)	2
*63	133.702	8.6±0.6	1.94±0.04	1.09±0.03	1	1.5	
64	136.64	2.2±0.7	1.48±0.06	1.12±0.19	(2)	(1.5)	
*65	137.63	2033±8	2.9±0.8	2.9±0.8	0	0.5	3
66	137.85	0.31	0.22±0.04	0.77	(1)	(0.5)	2
67	140.00	2.1±0.6	0.91±0.05	0.58±0.06	(1)	(1.5)	
*68	140.31	3091±10	0.9±0.6	0.9±0.6	0	0.5	3
69	140.76	0.31	0.22±0.4	0.77	(1)	(0.5)	2
*70	141.895	37.5±2.1	0.55±0.05	0.56±0.05	1	0.5	
71	142.43	1.1	1.86±0.07	1.4	(2)	(2.5)	2
72	143.13	0.25	0.19±0.06	0.77	(1)	(0.5)	2
*73	145.253	89.8±1.3	3.57±0.10	1.82±0.05	1	1.5	
*74	148.818	82.6±1.1	0.99±0.05	0.50±0.03	1	1.5	
*75	149.17	3.1±0.5	1.29±0.04	0.82±0.05	2	(1.5)	
*76	151.38	23.0±1.3	1.05±0.04	1.10±0.04	1	0.5	
77	155.44	0.46	0.29±0.03	0.77	(1)	(0.5)	2
*78	156.996	37.7±1.1	1.40±0.06	0.71±0.03	1	1.5	
*79	158.13	5246±13	3.3±0.8	3.3±0.8	0	0.5	3
80	159.87	8.0±2.4	2.13±0.06	1.23±0.07	2	(1.5)	
*81	161.29	16.2±1.0	3.20±0.07	1.14±0.03	2	(2.5)	
82	161.95	0.33	0.23±0.03	0.77	(1)	(0.5)	2
*83	166.08	52.1±2.0	0.36±0.05	0.36±0.05	1	0.5	
*84	167.10	16.5±1.0	2.17±0.06	1.16±0.03	2	(1.5)	
85	168.61	7.1±2.1	1.44±0.07	0.80±0.05	1	1.5	
*86	168.964	420±4	1.3±0.2	1.3±0.2	0	0.5	3
87	172.53	6.6±0.7	2.77±0.07	1.07±0.04	2	(2.5)	
*88	175.241	50.8±1.2	1.47±0.07	0.75±0.04	1	1.5	
89	176.16	5.0	0.51±0.05	0.57	(0)	(0.5)	2
*90	180.655	19.7±0.8	1.24±0.05	0.64±0.03	2	(1.5)	
*91	181.299	23.3±1.1	0.69±0.04	0.71±0.04	1	0.5	
92	183.94	7.0±0.5	1.78±0.05	1.02±0.03	2	(1.5)	
*93	184.606	107.9±1.1	1.61±0.06	0.81±0.03	1	1.5	
*94	185.50	3.1±0.3	2.33±0.05	1.03±0.05	2	(2.5)	
*95	185.995	26.2±0.7	1.19±0.05	0.61±0.03	1	1.5	
96	186.86	0.52	0.31±0.04	0.77	(1)	(0.5)	2
97	187.68	0.71	0.37±0.04	0.77	(1)	(0.5)	2
98	189.41	1.5±0.5	1.40±0.06	1.3±0.4	(2)	(1.5)	
99	191.48	9.3±0.6	1.63±0.07	0.90±0.04	2	(1.5)	
*100	191.913	2479±8	3.3±0.5	3.3±0.5	0	0.5	3
101	192.65	0.42	0.27±0.05	0.77	(1)	(0.5)	2
102	194.01	0.81	0.79±0.05	0.77	(1)	(1.5)	2
103	196.345	9.2±0.7	0.91±0.06	0.48±0.03	1	1.5	
*104	198.162	10.15±0.45	4.56±0.10	1.79±0.05	2	(2.5)	
105	200.55	0.37	0.25±0.05	0.77	(1)	(0.5)	2
106	201.49	4.7±1.4	1.02±0.05	0.57±0.04	(1)	(1.5)	
107	202.518	16.6±1.0	0.40±0.05	0.41±0.05	1	(0.5)	
*108	206.61	7438±17	6.9±1.0	6.9±1.0	0	0.5	3
*109	207.263	177.0±2.7	1.41±0.08	0.71±0.04	1	1.5	

TABLE II. (Continued).

	E_0 (keV)	Γ_n (eV)	$g\Gamma_n\Gamma_\gamma/\Gamma$ (eV)	Γ_γ (eV)	l^a	J^a	Notes
110	209.31	1.30	1.35±0.06	1.4	(2)	1.5	2
111	209.89	0.56	0.65±0.05	0.77	(1)	(1.5)	2
*112	211.043	60.7±1.7	0.75±0.06	0.76±0.06	0	0.5	
113	216.42	2.5±0.8	1.69±0.10	1.28±0.24	(2)	(1.5)	
114	216.55	8.0±1.0	2.42±0.11	1.43±0.08	2	(1.5)	
*115	216.69	212.9±3.8	0.50	0.50	1	0.5	
116	216.91	5.0±0.5	0.33	0.35	(1)	(0.5)	
117	217.92	6.5±0.7	0.89±0.15	0.49±0.09	2	(1.5)	
*118	218.123	18.0±0.8	1.88±0.16	0.99±0.09	1	1.5	
119	219.29	1.14	0.46±0.06	0.77	(1)	(0.5)	2
120	220.34	4.5±0.5	3.87±0.11	1.81±0.11	2	2.5	
121	224.35	1.60	1.48±0.06	1.4	(2)	(1.5)	2
122	229.40	1.5±0.2	2.84±0.09	2.6±0.6	(2)	(2.5)	
*123	231.104	44.5±0.7	1.39±0.08	0.71±0.04	1	1.5	
124	232.53	8.0±0.8	0.93±0.07	0.50±0.04	2	(1.5)	
*125	233.06	5654±13	5.3±0.7	5.3±0.7	0	0.5	3
126	233.61	0.47	0.29±0.06	0.77	(1)	(0.5)	2
*127	234.137	24.9±1.2	1.45±0.09	0.75±0.05	1	(1.5)	
128	235.38	0.64	0.35±0.07	0.77	(1)	(0.5)	2
129	236.82	0.66	0.71±0.15	0.77	(1)	(1.5)	2
130	237.00	0.55	0.64±0.15	0.77	(1)	(1.5)	2
131	241.10	1.6	0.52±0.06	0.77	(1)	(0.5)	2
132	242.36	2.6	0.61±0.08	0.80	(0)	(0.5)	2
133	242.772	27.3±1.0	1.31±0.09	0.67±0.05	1	1.5	
134	243.95	11.7±0.6	3.27±0.09	1.22±0.04	2	2.5	
135	245.09	7.0±2.1	0.37	0.39	(1)	(0.5)	
136	245.24	15±1.7	0.70±0.14	0.36±0.07	(1)	(1.5)	
137	245.39	20±2.4	0.49	0.50	(1)	(0.5)	
*138	245.553	237.6±2.7	0.55	0.55	0	0.5	
*139	245.63	21.3±1.6	2.41±0.24	1.28±0.12	2	(1.5)	
140	245.88	3.0±0.9	0.71	0.40	2	(1.5)	
141	249.24	0.44	0.28±0.06	0.77	(1)	(0.5)	2
*142	249.549	171.7±1.7	0.68±0.09	0.34±0.05	1	1.5	
*143	250.793	34.5±1.1	1.55±0.07	0.79±0.04	2	(1.5)	
144	254.28	28.6±1.5	0.97±0.08	1.01±0.09	1	(0.5)	
145	254.60	4.0±0.6	0.44	0.49	(1)	(0.5)	
146	255.09	7.6±0.7	2.24±0.09	1.31±0.07	1	(1.5)	
147	257.65	11.5±0.6	1.84±0.08	1.00±0.05	2	(1.5)	
*148	259.18	27.8±1.3	0.57±0.12	0.58±0.12	1	0.5	
*149	259.567	25.1±0.7	2.25±0.15	0.77±0.05	2	2.5	
150	260.28	3.7±0.6	2.69±0.10	1.18±0.08	2	(2.5)	
*151	261.93	15.2±0.9	0.98±0.08	1.05±0.09	0	0.5	
152	263.32	0.37	0.25±0.05	0.77	(1)	(0.5)	2
153	265.59	10.1±0.6	1.69±0.09	0.92±0.05	1	1.5	
*154	267.910	49.4±1.3	0.40±0.10	0.40±0.10	1	0.5	
*155	269.496	30.6±0.7	0.98±0.07	0.50±0.04	1	1.5	
*156	272.52	5449±13	5.4±0.6	5.4±0.6	0	0.5	3
*157	273.66	27.5±1.2	2.99±0.10	1.58±0.05	2	(1.5)	
158	275.71	0.92	0.42±0.08	0.77	(1)	(0.5)	2
*159	277.50	36.9±1.3	1.08±0.07	0.55±0.04	2	1.5	
*160	278.641	78.6±1.4	1.49±0.07	0.75±0.04	1	1.5	
161	281.27	1.65	1.05±0.11	0.77	(1)	(1.5)	2
*162	281.605	1986±8	1.75±0.40	1.75±0.40	0	0.5	3
163	284.70	2.3±0.7	1.31±0.08	0.92±0.14	(1)	(1.5)	
164	285.38	3.5	0.78±0.10	1.0	(0)	(0.5)	2
165	286.01	1.0±0.3	1.94±0.10	1.8±1.0	(2)	(2.5)	
*166	289.493	108.6±1.6	1.23±0.15	0.62±0.08	1	1.5	
167	289.95	7.8±0.6	4.33±0.17	1.77±0.09	2	(2.5)	
168	291.37	11.5±1.0	0.48±0.10	0.50±0.11	1	(0.5)	
169	292.93	6.6±0.7	2.09±0.09	1.24±0.07	2	(1.5)	

TABLE II. (Continued).

	E_0 (keV)	Γ_n (eV)	$g\Gamma_n\Gamma_\gamma/\Gamma$ (eV)	Γ_γ (eV)	l^a	J^a	Notes
170	295.39	3.9±1.2	1.50±0.08	0.93±0.09	(1)	(1.5)	
171	297.65	17.0±0.9	2.45±0.13	1.32±0.08	2	(1.5)	
172	298.09	1.35	0.49±0.11	0.77	(1)	(0.5)	2
173	299.44	1.7	0.53±0.09	0.77	(1)	(0.5)	2
*174	300.210	17.9±0.7	4.23±0.15	1.53±0.06	2	2.5	
*175	301.34	26.2±1.0	0.79	0.40	1	1.5	
*176	301.64	48.4±1.1	2.45±0.11	1.26±0.06	2	1.5	
177	304.85	2.5±0.8	0.34	0.40	(1)	(0.5)	
*178	305.21	98.8±1.2	2.27±0.34	1.15±0.17	2	(1.5)	
*179	305.405	666±5	2.8±0.5	2.8±0.5	0	0.5	3
180	307.33	11.0±1.2	1.43±0.10	1.64±0.13	1	(0.5)	
*181	307.468	180.0±3.2	0.70	0.70	1	0.5	
182	311.99	6.4±0.5	1.95±0.10	1.15±0.07	2	(1.5)	
183	313.00	1.9±0.6	1.47±0.23	1.2±0.4	(2)	(1.5)	
184	313.32	4.4±0.4	1.34±0.21	0.79±0.15	(1)	(1.5)	
*185	317.203	38.7±1.0	1.85±0.11	0.95±0.06	1	1.5	
186	321.32	21.6±0.8	1.87±0.25	0.98±0.13	2	(1.5)	
187	321.59	2.0±0.6	1.03±0.23	0.69±0.22	(1)	(1.5)	
188	325.18	4.4±0.3	1.43±0.12	0.85±0.09	1	(1.5)	
189	325.71	20±6	0.49	0.50	1	(0.5)	
190	325.88	24.0±1.5	2.05±0.22	1.07±0.12	1	1.5	
*191	326.021	1597±7	0.4	0.4	0	0.5	3
192	329.65	20.3±0.9	1.44±0.11	0.75±0.06	1	1.5	
193	332.91	0.68	0.72±0.09	0.77	(1)	(1.5)	2
*194	334.893	327.1±2.1	1.00	0.50	1	1.5	
*195	335.19	141.8±2.9	2.49±0.13	2.54±0.13	0	0.5	
196	336.00	0.97	1.72±0.11	1.4	(2)	(2.5)	2
197	337.60	4.0±0.8	1.20±0.10	0.71±0.07	2	(1.5)	
198	338.02	0.61	0.85±0.09	1.4	(2)	(1.5)	2
199	341.17	8.0±0.6	2.58±0.14	1.54±0.10	(2)	(1.5)	
200	342.67	9.0±0.6	4.48±0.18	1.79±0.09	2	(2.5)	
*201	343.571	100.9±1.3	2.02±0.24	1.02±0.12	1	1.5	
*202	344.331	109.8±1.3	4.00±0.22	2.04±0.11	2	1.5	
203	346.49	3.8±1.1	3.6±0.8	1.8±0.6	(2)	(2.5)	
204	346.60	2.5±0.8	2.8±0.8	1.5±0.7	(2)	(2.5)	
*205	349.66	1798±8	0.8±0.5	0.8±0.5	0	0.5	3
206	355.29	1.3	2.15±0.15	1.6	(2)	(2.5)	2
207	357.44	0.75	0.76±0.15	0.77	(1)	(1.5)	2
*208	357.786	161.8±1.6	1.20±0.25	0.60±0.13	1	1.5	
*209	359.92	63.7±1.2	1.58±0.22	0.80±0.11	2	(1.5)	
210	360.16	6.0±0.6	1.01	0.55	(1)	(1.5)	
211	360.63	29.0±1.0	2.96±0.21	1.56±0.12	1	(1.5)	
212	363.46	12.5±0.8	2.42±0.14	1.34±0.09	2	(1.5)	
213	364.38	8.0±0.5	2.37±0.16	0.88±0.07	2	(2.5)	
*214	365.37	34.6±1.1	1.87±0.15	0.96±0.08	1	1.5	
*215	367.737	129.6±2.2	0.40	0.40	0	0.5	
216	368.03	1.6	1.48±0.13	1.4	(2)	(1.5)	2
217	370.12	8.0±0.6	2.14±0.15	1.24±0.10	2	(1.5)	
*218	371.217	55.0±1.1	1.93±0.16	0.98±0.08	1	1.5	
219	374.03	1.5	1.02±0.13	0.77	(1)	(1.5)	2
220	376.34	11.5±0.9	1.19±0.17	0.63±0.09	2	(1.5)	
221	376.76	0.53	1.15±0.23	1.4	(2)	(2.5)	2
222	377.14	37.8±1.0	1.18±0.18	0.60±0.09	1	1.5	
*223	379.002	80.0±1.0	5.29±0.21	1.80±0.07	2	2.5	
*224	379.947	229.7±3.4	0.90±0.19	0.90±0.19	1	0.5	
225	384.55	6.0±0.6	3.83±0.14	1.62±0.09	2	(2.5)	
226	390.02	9.2±1.0	1.86±0.14	1.04±0.09	1	1.5	
227	391.57	0.88	1.08±0.13	1.4	(2)	(1.5)	2
*228	395.030	693±5	0.50	0.50	0	0.5	
229	395.10	16±5	1.52±0.09	0.80±0.05	2	(1.5)	

TABLE II. (Continued).

	E_0 (keV)	Γ_n (eV)	$g\Gamma_n\Gamma_\gamma/\Gamma$ (eV)	Γ_γ (eV)	l^a	J^a	Notes
*230	395.34	29.3±1.1	3.04±0.16	1.05±0.06	2	(2.5)	
231	395.66	14±4	0.48	0.50	(1)	(0.5)	
*232	397.403	150.1±2.3	1.94±0.35	0.98±0.18	1	1.5	
*233	397.85	275±5	1.02±0.35	1.02±0.35	1	0.5	
234	400.65	10.0±0.8	1.29±0.14	0.69±0.08	2	(1.5)	
235	401.11	1.0	2.06±0.25	2.20	(2)	(2.5)	2
236	405.95	17.3±0.8	0.96±0.17	0.49±0.09	1	1.5	
*237	407.017	47.2±1.1	0.99	0.50	2	(1.5)	
238	408.23	6±2	0.36	0.38	(1)	(0.5)	
239	408.49	11.0±0.8	2.05±0.18	1.13±0.11	2	(1.5)	
*240	409.55	70.1±1.9	0.50	0.50	1	0.5	
241	410.02	20.8±0.7	3.22±0.19	1.13±0.07	2	(2.5)	
242	411.31	2.3±0.7	0.43	0.53	(1)	(0.5)	
*243	413.551	97.4±1.2	1.61±0.20	0.81±0.10	1	1.5	
244	414.74	3.2±1.0	2.38±0.17	1.05±0.15	(2)	(2.5)	
*245	416.319	263.1±2.2	4.70±0.24	2.37±0.12	1	1.5	
*246	417.56	9297±29	2.6±1.4	2.6±1.4	0	0.5	3
247	420.65	35.6±1.4	1.52±0.19	0.78±0.10	1	1.5	
*248	424.68	7920±29	3.3±1.8	3.3±1.8	0	0.5	3
249	425.40	12.0±1.0	2.43±0.22	1.35±0.14	2	(1.5)	
250	425.96	24.0±2.0	0.87	0.90	(1)	(0.5)	
*251	426.79	120.9±1.5	1.79±0.24	0.60±0.08	2	(2.5)	
*252	428.058	1152±15	0.9±0.6	0.9±0.6	0	0.5	3
253	428.70	9.5±3.0	1.43±0.24	0.77±0.14	2	(1.5)	
*254	429.85	52.6±1.2	6.0±0.3	2.08±0.11	2	2.5	
255	431.78	4.0±1.4	1.06	0.61	(1)	(1.5)	
256	433.097	112.2±2.1	1.34±0.16	0.67±0.08	1	1.5	
257	434.82	7.6±2.3	2.36±0.24	1.40±0.19	(2)	(1.5)	
*258	435.03	377±6	1.0	1.0	1	0.5	
259	435.90	58.2±1.4	5.3±0.3	1.83±0.11	2	(2.5)	
*260	436.604	111.2±2.0	3.00	1.50	1	1.5	
*261	439.23	71.6±1.7	2.00	1.00	2	1.5	
262	439.52	2.9±0.9	2.91±0.20	1.46±0.27	(2)	(2.5)	
263	441.80	0.75	0.38±0.10	0.77	(1)	(0.5)	2
264	443.55	2.7	1.20±0.17	0.77	(1)	(1.5)	2
265	444.95	5.0±1.5	2.71±0.20	1.10±0.12	(2)	(2.5)	
*266	446.971	113.9±1.4	3.16±0.21	1.06±0.07	2	2.5	
*267	452.188	187.7±2.1			1	1.5	
268	455.09	6.0±2.0			(1)	(0.5)	
*269	455.50	1866±12			0	0.5	
*270	455.54	39.3±2.0			1	1.5	
271	457.54	42.0±1.2			2	(2.5)	
*272	459.667	287.3±3.0			1	1.5	
*273	462.258	458±5			0	0.5	
*274	463.310	151.2±2.2			2	1.5	
275	466.17	18.2±1.2			1	(1.5)	
*276	469.259	175.1±2.4			1	1.5	
*277	470.414	489±7			0	0.5	
278	476.070	52.2±1.2			2	2.5	
279	477.28	164.6±3.6			1	0.5	
280	479.90	39.3±1.1			2	2.5	
281	482.73	14.0±1.2			2	(1.5)	
282	485.78	9.0±2.7			(1)	(1.5)	
283	487.14	19.0±1.3			2	(1.5)	
284	487.62	16±5			(1)	(0.5)	
*285	491.47	91.7±2.2			1	1.5	
*286	491.816	182±5			0	0.5	
*287	493.171	386±8			1	0.5	
*288	493.741	91.6±1.8			2	(2.5)	
289	495.32	9.4±2.8			(2)	(1.5)	

TABLE II. (Continued).

	E_0 (keV)	Γ_n (eV)	$g\Gamma_n\Gamma_\gamma/\Gamma$ (eV)	Γ_γ (eV)	l^a	J^a	Notes
290	496.03	15±5			(1)	(0.5)	
*291	496.32	1415±10			0	0.5	
292	496.38	31±9			(1)	(0.5)	
*293	496.84	241±5			1	0.5	
294	498.93	25.5±1.5			1	(1.5)	
295	503.85	35.4±1.1			2	(2.5)	
296	506.86	35.5±1.2			2	(1.5)	
297	507.64	26.2±2.6			(1)	(0.5)	
*298	507.78	1551±10			0	0.5	
*299	508.24	79.7±2.6			2	(1.5)	
*300	508.59	62.2±2.5			2	(1.5)	
*301	508.86	54.6±2.2			1	1.5	
302	509.50	10.5±3.2			2	(1.5)	
*303	511.205	145.7±2.0			1	1.5	
*304	513.359	181.5±2.1			1	1.5	
305	513.97	15±5			2	(2.5)	
306	514.38	10.5±3.2			2	(2.5)	
307	515.89	5.7±1.7			(2)	(1.5)	
308	518.471	49.5±1.1			2	2.5	
309	520.80	12.5±3.8			(1)	(0.5)	
*310	521.70	117.9±3.1			1	0.5	
311	523.25	9.1±2.7			(1)	(0.5)	
*312	523.54	1294±9			0	0.5	
*313	524.08	68.4±1.5			2	2.5	
314	527.83	48.7±1.2			2	2.5	
*315	529.25	203.2±3.7			0	0.5	
*316	529.42	81.4±2.0			1	1.5	
317	530.68	27.0±1.0			2	(2.5)	
*318	539.859	86.4±1.7			2	(1.5)	
319	540.53	14±4			(1)	(0.5)	
*320	541.213	519±7			0	0.5	
*321	541.89	46.4±2.0			1	1.5	
322	543.73	18.1±1.1			2	(2.5)	
323	544.82	36.6±1.1			2	(2.5)	
324	545.81	30.1±2.2			(1)	(0.5)	
325	547.88	47.0±1.4			1	1.5	
326	550.17	54.1±1.5			2	(1.5)	
327	552.12	16±5			(1)	(0.5)	
*328	552.53	75.3±1.5			1	1.5	
*329	553.73	2409±15			0	0.5	
330	553.89	30.5±3.0			2	(1.5)	
*331	555.57	64.5±2.0			1	1.5	
332	558.30	8.9±2.7			(2)	(1.5)	
*333	559.733	852±14			0	0.5	
*334	560.427	366±9			1	0.5	
335	566.36	28.7±2.0			2	(1.5)	
336	567.72	7.9±2.4			(1)	(0.5)	
*337	567.82	9282±34			0	0.5	
*338	569.55	56.5±1.8			2	(1.5)	
339	574.19	41.8±1.3			2	(2.5)	
*340	575.892	409.8±3.5			1	1.5	
341	582.54	33.9±1.2			2	2.5	
*342	585.55	180±4			1	0.5	
*343	587.693	98.6±1.3			2	2.5	
*344	588.85	2315±14			0	0.5	
345	591.85	43.0±2.0			1	1.5	
*346	595.60	126.8±2.0			1	1.5	
347	598.52	6.8±2.0			(1)	(0.5)	
348	599.46	45.4±1.5			2	(1.5)	
349	600.15	11.3±3.4			(1)	(0.5)	

TABLE II. (Continued).

	E_0 (keV)	Γ_n (eV)	$g\Gamma_n\Gamma_\gamma/\Gamma$ (eV)	Γ_γ (eV)	l^a	J^a	Notes
*350	600.69	8070±30			0	0.5	
*351	601.526	225.5±3.1			2	1.5	
*352	604.399	316.4±2.5			2	2.5	
*353	609.439	207.6±2.7			2	1.5	
*354	610.978	271.3±2.3			2	2.5	
355	612.47	23±7			(1)	(0.5)	
356	613.25	45±5			(1)	(0.5)	
357	613.60	23±7			(1)	(0.5)	
358	614.25	30±9			(1)	(0.5)	
359	616.51	39.0±2.0			2	(1.5)	
360	617.19	19±6			(1)	(0.5)	
*361	618.20	404±6			0	0.5	
362	618.31	30.7±3.1			2	(1.5)	
363	622.17	57.5±1.5			2	(2.5)	
364	625.08	109.3±2.3			1	1.5	
*365	627.107	1011±8			2	1.5	
*366	628.38	448±10			1	0.5	
*367	629.59	95.4±2.2			1	1.5	
*368	630.96	150±9			0	0.5	
*369	631.74	371±21			1	0.5	
*370	631.96	78±7			1	(1.5)	
*371	633.041	342.1±2.8			2	2.5	
*372	635.73	81.6±2.1			(1)	(1.5)	
*373	636.42	9340±44			0	0.5	
*374	636.45	46.2±1.4			2	(2.5)	
*375	637.08	126.2±2.6			2	(1.5)	
*376	640.45	84.2±1.8			2	(2.5)	
*377	644.05	44.6±1.6			2	(2.5)	
378	644.35	15±4			(1)	(1.5)	
*379	646.04	162±5			1	0.5	
*380	649.76	169.6±2.6			2	(2.5)	
*381	650.562	525±5			1	1.5	
*382	654.966	348.6±3.7			2	1.5	
383	656.84	17±5			(2)	(1.5)	
*384	660.28	1218±12			0	0.5	
*385	661.12	537±9			1	0.5	
386	664.94	16±5			(2)	(1.5)	
*387	665.508	229.1±3.0			1	1.5	
*388	667.84	149.5±2.3			2	(1.5)	
389	668.60	11.0±3.3			(1)	(1.5)	
*390	670.19	5411±29			0	0.5	
*391	670.65	203.0±2.7			2	2.5	
*392	672.81	234.1±3.2			1	1.5	
393	673.61	89.0±2.0			2	(2.5)	
*394	675.00	232.5±3.2			2	1.5	
*395	677.49	97.5±2.4			2	1.5	
396	678.58	42.5±2.0			2	(1.5)	
397	680.65	65.4±2.1			2	(1.5)	
398	681.65	51.5±2.0			1	1.5	
*399	686.74	229±6			1	0.5	
400	690.32	71.4±2.5			1	1.5	
*401	691.259	540±5			2	1.5	
402	692.55	54±16			(1)	(0.5)	
*403	693.00	98.5±4.0			2	(1.5)	
*404	693.556	314.8±3.7			2	2.5	
*405	695.56	870±19			0	0.5	
*406	696.16	391±5			1	1.5	
407	698.03	28±8			2	(1.5)	
*408	699.10	1232±15			0	0.5	
409	700.77	20±6			1	(0.5)	

TABLE II. (Continued).

	E_0 (keV)	Γ_n (eV)	$g\Gamma_n\Gamma_\gamma/\Gamma$ (eV)	Γ_γ (eV)	I^a	J^a	Notes
*410	703.12	1150±16			1	0.5	
*411	705.49	413±8			1	0.5	
*412	707.083	337±4			1	1.5	
*413	708.435	395±4			2	1.5	
*414	710.97	212.0±3.0			2	1.5	
*415	712.39	119±5			1	0.5	
416	712.80	9±3			(1)	(1.5)	
417	713.10	18±5			1	(0.5)	
*418	714.70	108.0±1.7			2	(2.5)	
*419	715.71	138.0±2.5			1	(1.5)	
420	718.62	18.2±2.0			2	(1.5)	
*421	719.71	59.9±1.7			2	(2.5)	
*422	720.33	5313±38			0	0.5	
*423	720.94	94.3±3.4			(1)	(1.5)	
424	723.05	8.5±2.6			(2)	(1.5)	
425	728.15	24±7			2	(1.5)	
*426	731.70	85±9			(0)	(0.5)	
*427	732.14	218±4			2	1.5	
*428	732.75	12.4±2.6			(1)	(0.5)	
*429	734.00	78±4			2	(2.5)	
*430	734.15	453±8			2	1.5	
431	735.50	18±5			(1)	(0.5)	
*432	737.26	83.3±2.2			2	(1.5)	
*433	738.26	3582±40			0	0.5	
434	740.10	32±10			(1)	(0.5)	
*435	740.91	289±7			1	0.5	
436	744.44	18±5			(1)	(1.5)	
*437	745.202	440±4			2	1.5	
*438	746.27	279±4			2	1.5	
439	746.37	32±10			2	(2.5)	
440	746.87	27±8			(2)	(1.5)	
*441	748.15	21665±102			0	0.5	
442	747.97	34.9±3.0			(2)	(2.5)	
443	749.50	24±7			(1)	(0.5)	
*444	749.95	173.2±3.1			1	1.5	
445	750.40	15±5			(2)	(1.5)	
*446	751.73	179±5			2	(1.5)	
*447	752.16	132.0±3.1			2	(2.5)	
*448	753.70	1289±28			0	0.5	
449	759.01	115±5			1	0.5	
450	759.98	40±12			(1)	(0.5)	
451	761.06	59.0±2.5			2	(1.5)	
*452	762.29	234±7			1	0.5	
453	764.11	31±5			(2)	(1.5)	
454	765.05	68.0±2.7			1	(1.5)	
*455	768.76	4264±26			0	0.5	
*456	775.16	445±9			0	0.5	
*457	776.06	469±5			2	1.5	
*458	778.27	93.3±2.3			2	(2.5)	
*459	780.03	119.6±2.5			2	(2.5)	
460	781.42	20±6			(1)	(1.5)	
*461	782.15	197.6±3.1			2	1.5	
*462	784.00	209.2±3.3			1	1.5	
*463	784.76	7466±46			0	0.5	
464	789.31	20±6			(1)	(0.5)	
465	790.40	23±7			(1)	(0.5)	
*466	791.16	168.2±2.4			2	(2.5)	
*467	792.61	267.5±4.0			2	1.5	
468	793.40	72.0±3.0			1	(1.5)	
469	795.80	44±7			(1)	(0.5)	

TABLE II. (Continued).

	E_0 (keV)	Γ_n (eV)	$g\Gamma_n\Gamma_\gamma/\Gamma$ (eV)	Γ_γ (eV)	l^a	J^a	Notes
*470	796.42	68.4 ± 2.7			1	1.5	
471	797.45	25 ± 8			(1)	(0.5)	
*472	798.59	5111 ± 40			0	0.5	
*473	800.66	262.4 ± 3.3			2	2.5	
*474	801.46	100.3 ± 3.4			2	1.5	
475	802.70	37 ± 11			(0)	(0.5)	
476	804.82	34.5 ± 2.3			1	(1.5)	
477	806.96	46.2 ± 2.9			1	1.5	
478	809.29	133.9 ± 2.6			(2)	(2.5)	
479	811.05	39 ± 12			(1)	(0.5)	
*480	821.5	$(11.2\pm 0.2)\times 10^3$			0	0.5	1
*481	868	$(4.1\pm 1.8)\times 10^3$			0	0.5	1
*482	1000	$(227\pm 3)\times 10^3$			0	0.5	1

^aParentheses are used to indicate that the assignment is uncertain.

data could be analyzed with energy-independent radii if a smaller radius is used for p -wave than for s - and d -wave resonances. These two radii were adjusted by the code; a good fit to the data was achieved with the p -wave radius equal to 4.23 ± 0.01 fm and the radius for s - and d -wave resonances equal to 6.29 ± 0.01 fm.

During the process of fitting the transmission data with the code SAMMY, a normalization factor and a background correction, both energy independent, were allowed to be adjusted for each data set. Background corrections to the transmission data are less than 0.008, and all three normalization factors are unity within 1%.

The transmission data from 0.1 to 813 keV are well described with 421 resonances, of which two are negative-energy resonances and three are above the analyzed region. These five external resonances do not correspond to actual resonances in ^{58}Ni , but were used to describe accurately the smooth cross section in the region analyzed; therefore, these resonances must be included for the correct description of the data in this energy region. The

thermal total cross section generated from the ^{58}Ni parameters of Table II is equal to 29.4 b, which is in good agreement with the value of 29.9 ± 0.6 b recommended in Ref. [29] for the sum of the thermal neutron scattering and capture cross sections.

Capture data were analyzed concurrently with the transmission data up to 450 keV. All the resonances seen in the transmission data were also seen in the capture data, but 61 resonances analyzed in the capture data had neutron widths too small for the resonances to be detected in transmission; however, these resonances were included in the transmission calculation to verify that the neutron widths assigned to these resonances are consistent with the transmission data.

All resonances showing the characteristic potential interference pattern of s waves were assigned as s waves. The differential elastic-scattering data were used to assign the spin and parity of $l > 0$ resonances whose neutron widths were large enough for them to be observed in the elastic-scattering data. Weak resonances were arbitrarily assigned as $p_{1/2}$ where evidence for a different assignment was lacking.

B. Capture data analysis

The corrected capture data were converted to effective cross section versus neutron energy and fitted to resonance parameters by a least-squares adjustment using the Breit-Wigner formula through the computer code LSFIT [30]. The program iterates upon trial parameters, applying corrections for energy resolution, Doppler width, self-shielding, and multiple scattering.

The corrections for self-shielding and multiple scattering done in LSFIT are approximate for some of the resonances analyzed in this paper. In order to test the validity of these corrections, exact calculations were made for the self-shielding of some ^{58}Ni resonances, using total cross sections based upon the analysis of the transmission data. Calculations were also made for the contributions due to capture following one elastic scattering, including angular distribution effects based upon the scattering

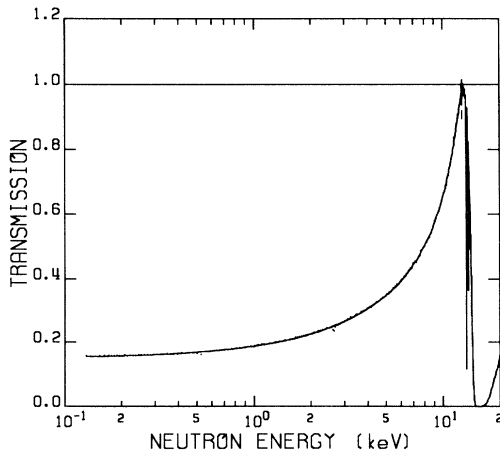


FIG. 1. Fit to the 78-m transmission data below 20 keV taken with the ^6Li -glass detector. The averaged data are barely distinguishable from the theoretical curve.

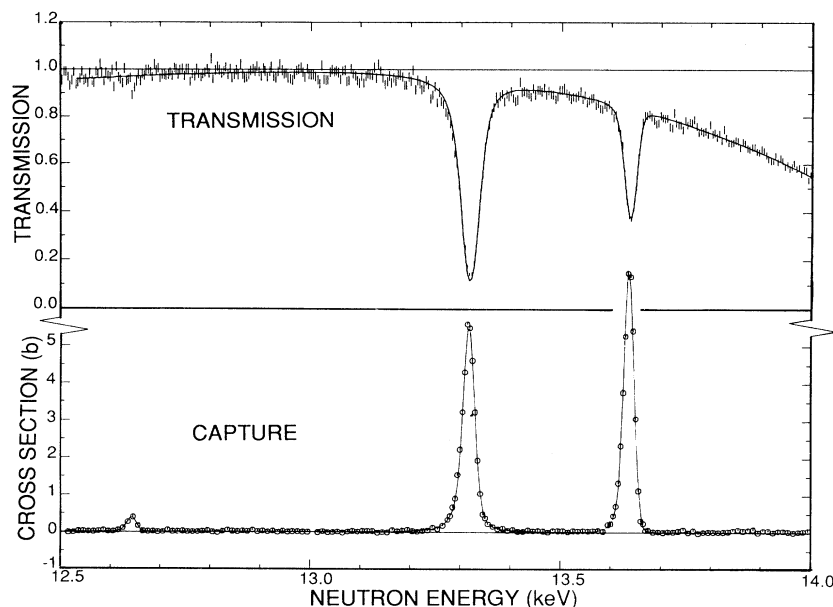


FIG. 2. 12.5–14-keV energy region is enlarged from Fig. 1 to show in detail the fit to the transmission data. The concurrent fit to the capture data taken with the thin sample is shown in the lower part of the figure.

data; but an approximation was used in treating capture following two elastic scatterings. The corrections calculated by LSFIT were found to be very good for isolated narrow resonances. However, in the vicinity of large s waves, the capture areas determined by LSFIT were found to be over- or underpredicted by as much as 10%.

The thin sample capture data were analyzed up to 22 keV, and the thick sample data were used between 22 and 450 keV. At still higher energies, average corrections for sample thickness were applied to the thick sample data to derive average neutron capture cross sections.

For resonances seen clearly in both capture and transmission data, energies and neutron widths were taken from the transmission data analysis. Between 5 and 450 keV, about 30% more resonances were seen in the capture data than in the transmission data. For these 61 resonances, only the resonance energies and the capture kernels, $g\Gamma_n\Gamma_\gamma/(\Gamma_n+\Gamma_\gamma)$, are defined. When possible, these resonances were given a p -wave assignment, the neutron width set to be consistent with the lack of observation in the transmission data, and the radiation width set equal to the average p -wave radiation width of 0.77 eV. However, because of their large capture areas, nine resonances were given a d -wave assignment with a radiation width of 1.4 eV. An s -wave assignment was given to three resonances, at 176.16, 242.36, and 285.38 keV, even though they were clearly seen only in the capture data; such an assignment gives better agreement with the transmission data than a $p_{1/2}$ assignment would.

Since the data showed a low-energy (i.e., time-delayed) tail on the usual Gaussian resolution function, a resolution shape modification was included in LSFIT. At 6 keV, 15% of the resolution function was in a low-energy tail, increasing to 50% at 200 keV. This asymmetric part is an exponential whose time decay constant is 69% of the FWHM of the Gaussian resolution function.

A correction for capture in the detector environment of neutrons scattered from discrete resonances in the

sample is required [31]. This prompt neutron sensitivity can be formulated as a correction to the radiation width such that $\Gamma_\gamma(\text{corr}) = \Gamma_\gamma - C\Gamma_n$, where C is dependent on the amount and distribution of absorber in the vicinity of the detector. The plot of this correction factor as a function of the incident neutron energy is shown in Fig. 3. It is based on measurements of the detector response to samples of carbon and ^{208}Pb . Peaks in the sensitivity curve correspond to neutron resonances in the fluorine of the C_6F_6 liquid scintillator, silicon in the quartz scintillator cell, and the aluminum housing around the sample and detector. The underlying nonresonant response was attributed in part to neutron capture by boron in the photomultiplier tubes. The uncertainty is $\approx 40\%$. Note 3 in Table II indicates the resonances for which the radiation widths and capture kernels were corrected for this effect.

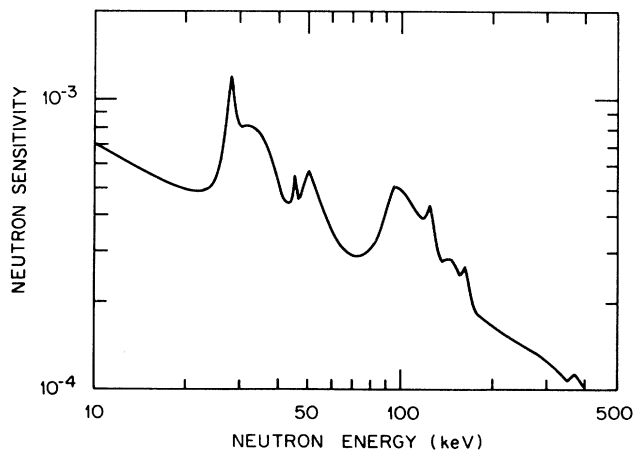


FIG. 3. Capture detector neutron sensitivity as a function of the incident neutron energy for the ^{58}Ni samples.

C. Differential elastic-scattering data analysis

The elastic-scattering measurements were used as the principal tool to determine the spin and parity of the $l > 0$ resonance above 30 keV. Theoretical calculations of the cross section at six scattering angles were compared with the experimental data, testing various combinations of spins and parities. The combination of spin and parity which yielded the best agreement with the data was adopted.

Theoretical cross sections were calculated as a function of incident neutron energy with the R -function code RFUNC [32], which is based on the Blatt-Biedenharn formalism [33]. Doppler broadening and experimental resolution are included, as are approximate corrections for attenuation and for multiple scattering in the sample.

Comparison of the experimental data for four elastic-scattering angles with theoretical calculations for the resonance at 82.88 keV (Fig. 4) illustrates how the spin and parity of a well-separated resonance, clearly seen in the transmission and differential elastic-scattering data, can be assigned without ambiguity. The two solid lines, for each of the four angles shown, are the theoretical curves obtained with an orbital angular momentum l equal to 1 and a spin of $\frac{1}{2}$ (thin line) or $\frac{3}{2}$ (thick line). The dashed line is obtained with $l=2$ and a spin of $\frac{3}{2}$. The three theoretical curves for the 39° angle do not display striking differences (the shapes are similar; only the positions and

the amplitudes are slightly different), whereas at 90° the shapes for the $l=1$ and 2 resonances are very different. From this observation on the 90° data, we can conclude that this is a p -wave resonance and, most likely, has a spin of $\frac{3}{2}$ since the thick line curve agrees much better with the data than does the thin one. At 90° , an important feature of the data is that $l=1$ resonances have a symmetrical shape about the resonance energy, whereas $l=2$ resonances have an asymmetrical shape. As was the case at 39° , the curves at 120° are not very different, but seem to confirm the $p_{3/2}$ assignment for this resonance. The theoretical calculations at 160° show (as was the case at 90°) a striking difference in the shape of the curves corresponding to $l=1$ and 2. The data at 160° are also in better agreement with the thick line curve than with the thin one. Therefore a $p_{3/2}$ assignment is adopted with a good degree of confidence.

The difference in the amplitudes at 39° , 90° , and 160° for a $p_{1/2}$ and a $p_{3/2}$ resonance is often large enough to distinguish between the two possible spins of a p -wave resonance. This is less often the case for d -wave resonances. For clarity, the theoretical curve calculated for a $d_{5/2}$ resonance is not shown on Fig. 4. At 39° , the curves for $d_{3/2}$ and $d_{5/2}$ resonances are almost indistinguishable. At 90° and 160° , the amplitudes are slightly larger for a $d_{5/2}$ than for a $d_{3/2}$ resonance. Only 30% of the assigned d -wave resonances, compared to 83% of the assigned p -wave resonances, could also have their spin assigned with some degree of confidence.

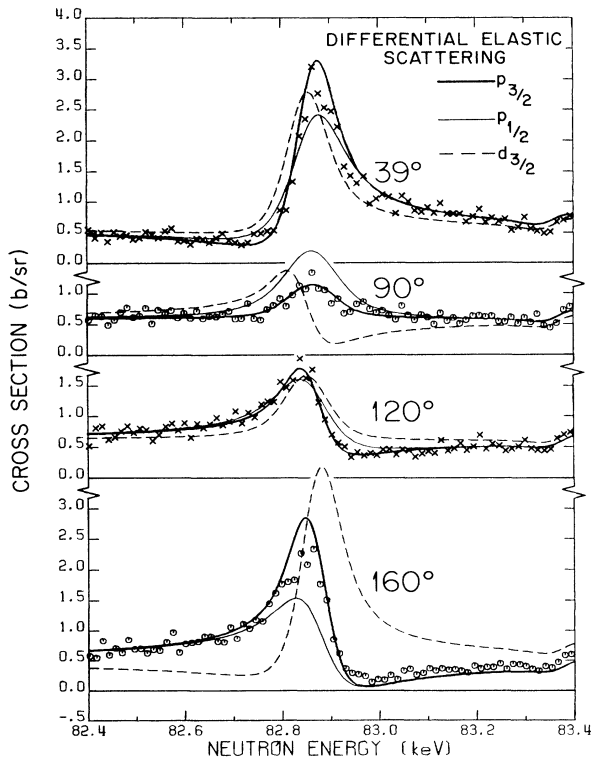


FIG. 4. Theoretical calculations with three different spin and parity assignments are compared with the data for four of the six elastic-scattering angles to illustrate that the $p_{3/2}$ assignment for this resonance is unequivocal.

IV. RESULTS AND DISCUSSION OF THE UNCERTAINTIES

The resonance parameters obtained from the concurrent analyses of the ^{58}Ni transmission, capture, and differential elastic-scattering data are given in Table II. Samples of fits to the transmission and capture data obtained with this set of resonance parameters and the comparison of the theoretical calculations with the differential elastic-scattering data are shown in Figs. 2 and 5–8.

In Table II parameters are reported for 477 resonances in the 0.1–813-keV energy range and for 5 fictitious resonances given outside that energy range (note 1). The resonance number is in the first column. An asterisk next to the resonance number indicates that the parameters of this resonance were among the 355 parameters that were adjusted in the final fit to the transmission data with the code SAMMY. The covariance matrix associated with these 355 adjusted parameters is available from the authors. The next four columns show the energies of the resonances, the neutron widths, the capture kernels, and the radiation widths followed by their uncertainty when available.

The orbital angular momentum l and the spin J for each resonance are given in columns 6 and 7. Parentheses indicate uncertain assignments. The numbers in the last column correspond to notes found at the end of the table.

Between 5 and 450 keV, where capture data were also analyzed, note 2 is used to indicate the 61 resonances too

weak to be detected in the transmission data but clearly seen in the capture data.

Uncertainties on the energy values are less than 0.005 keV when three decimal positions are specified for the energy and less than 0.05 keV when only two are specified. Uncertainties reported on the neutron widths are statistical uncertainties from the code SAMMY. A 20–30 % uncertainty on the neutron width of some of the narrow resonances indicates that these parameters were adjusted by trial and error. The uncertainties on the capture kernels were obtained from the capture fitting code LSFIT unless note 3 is present; note 3 indicates that, because of the large neutron width, the correction for the neutron sensitivity of the detector was important and its uncertainty was combined with the statistical uncertainty given by the code. The uncertainties on the radiation widths were propagated from the uncorrelated uncertainties on the neutron widths and on the capture kernels.

As noted earlier, comparison of the differential elastic-scattering data with the theoretical calculations allows us to assign spin and parity to many of the $l > 0$ resonances.

Between 30 and 813 keV, 353 $l > 0$ resonances were analyzed in the transmission data; 311 could be identified in the elastic-scattering data, but 46 were too weak to provide any information on spin or parity. Definite l assignments can be made for 265 resonances, i.e., for 75% of the $l > 0$ resonances seen in the transmission data above 30 keV (124 are p -wave and 141 are d -wave resonances.) The spin of 83% of the 124 p -wave resonances can be assigned with some degree of confidence (33 have spin $\frac{1}{2}$ and 70 spin $\frac{3}{2}$), but only 30% of the 141 d -wave resonances could be given a definite spin assignment (22 have spin $\frac{3}{2}$ and 21 spin $\frac{5}{2}$). It is interesting to note that among the p -wave resonances where a definite J assignment can be made there are twice as many resonances with J of $\frac{3}{2}$ than with J of $\frac{1}{2}$. This ratio is in agreement with the $(2J+1)$ weighting factor. Too few definite J assignments can be made in the case of d waves to draw conclusions regarding the ratio of the number of $d_{3/2}$ and $d_{5/2}$ resonances.

Considering all the $l > 0$ resonances given in Table II

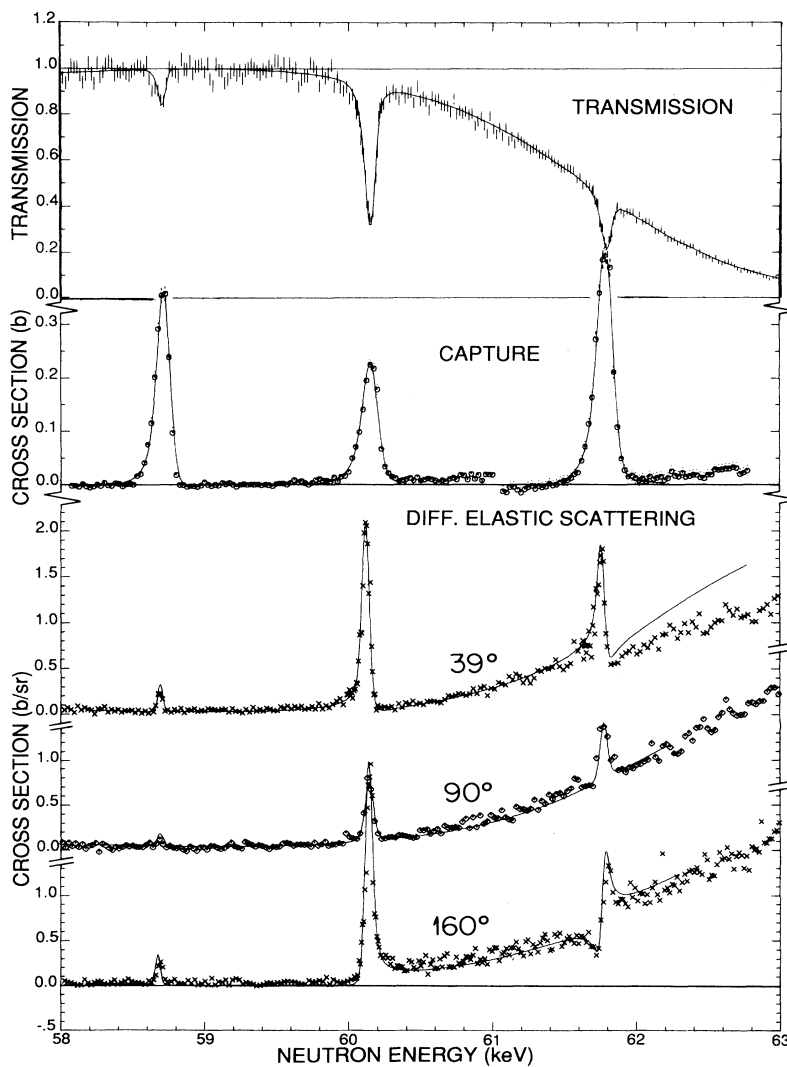


FIG. 5. Top: Concurrent fits, from 58 to 63 keV, to the 78-m transmission data taken with the NE-110 detector and to the capture data obtained with the thick ^{58}Ni sample. Bottom: The data for three of the six differential elastic-scattering angles are compared with the theoretical cross sections calculated with the parameters of Table II.

we find 238 assigned p -wave resonances and only 178 assigned d -wave resonances, whereas according to the $(2J+1)$ rule, with 61 s -wave resonances there should be 183 p -wave and 305 d -wave levels. The larger than predicted fraction of p -wave resonances assigned in Table II is a consequence of assigning many narrow resonances as p wave by default.

The thermal capture cross section reported by Mughabghab, Divadeenam, and Holden [29] for ^{58}Ni is 4.6 ± 0.3 b. The observed s -wave resonances contribute approximately 0.3 b; the difference of 4.3 b should be attributed to bound levels. The radiation widths of the two s -wave bound levels were chosen so that they generate the missing 4.3 b.

The ^{58}Ni resonance parameters of Table II also correctly predict the thermal total cross section as recommended in Ref. [29] (see Sec. III A).

V. COMPARISON WITH OTHER WORKS

Among the transmission data analyses reported earlier, the most extensive one is the Harwell data analysis [6,7] between 10 and 650 keV. The Harwell analysis of Syme, Bowen, and Gadd, along with an evaluation by Fröhner

[8] based on an analysis of capture yield measurements made at Karlsruhe [34], is compared with our results in the following sections. The Harwell and Fröhner sets of resonance parameters were extensively used by Mughabghab, Divadeenam, and Holden [29] in their ^{58}Ni resonance parameter evaluation. The capture measurements of Wisshak *et al.* [9] below 30 keV will also be discussed.

A. Comparison with Harwell resonance parameters

The Harwell transmission data [6] taken between 10 keV and a few MeV have an experimental resolution (0.075 ns/m) comparable to the resolution of our 78-m data (0.050 ns/m), but our data taken at the 200-m flight-path station have much better resolution (0.025 ns/m). For example, at 500 keV our resolution (FWHM) is 260 eV compared to ≈ 700 eV for the Harwell data.

The Harwell parameters for the s -wave resonances were taken from a subsequent report [7] where the data were analyzed with a single-channel multilevel R -matrix code in which an energy-dependent effective scattering radius was used. At 400 keV this radius was equal to about 6 fm.

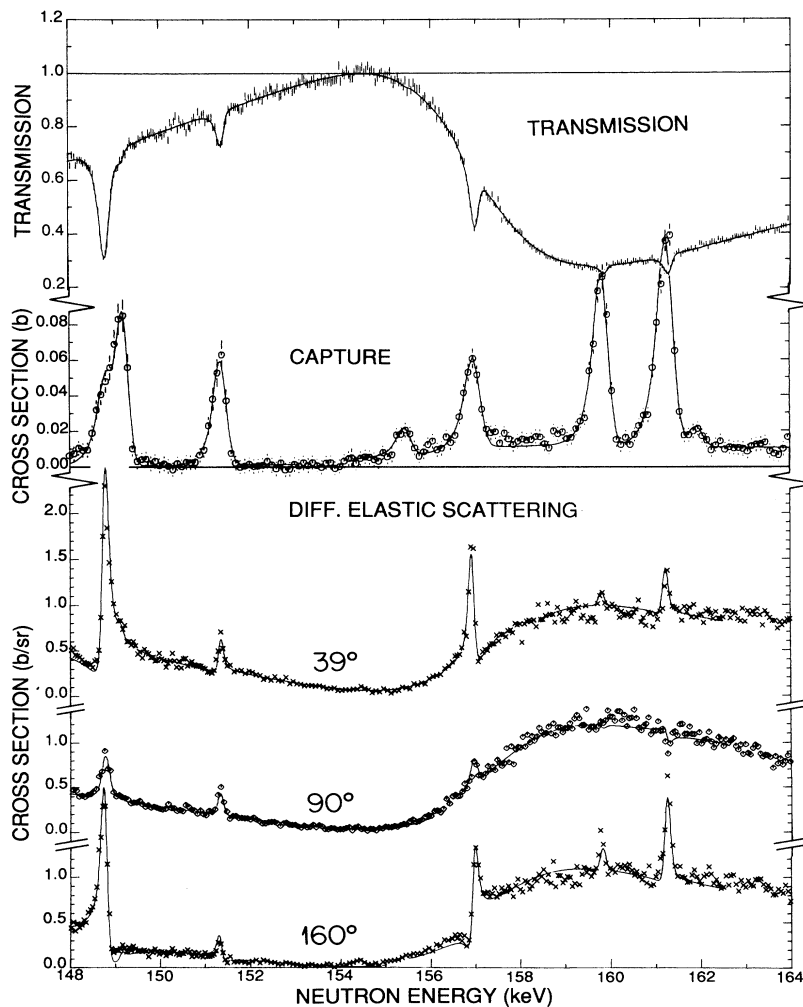


FIG. 6. Same as Fig. 5 except for 148–164 keV.

In Table III the energies and the neutron widths for the s -wave resonances reported in Table II are compared with the parameters of Syme and Bowen [7]. Eight of our 47 s -wave resonances below 650 keV are not seen by Syme and Bowen. Of these eight resonances, three are very weak in transmission, but are clearly seen in the capture data; their assignment as s -wave resonances is uncertain. The other five are clearly identified as s -wave resonances from our transmission data. Syme and Bowen report two s -wave resonances not seen in our data: The one at 172 keV is very small and has a large uncertainty; the one at 473.96 keV is interpreted in our data as an $l=2$ resonance at 476.07 keV. The resonance energies reported in this work are systematically higher by $\approx 0.2\%$ than the energies reported by Syme and Bowen. Our reported neutron widths are larger for 27 of the 39 s -wave resonances seen in both data sets.

The resonance parameters of the $l>0$ resonances reported by Syme and Bowen were obtained through an area analysis. The authors found 97 $l>0$ resonances between 10 and 650 keV compared to the 273 that we could see in our transmission data in the same energy interval. In a subsequent analysis [7], they mentioned that 230

$l>0$ resonances were analyzed with a multilevel R -matrix code between 10 keV and 1 MeV, but no values were reported for the parameters.

B. Comparison with Fröhner's evaluation

The Karlsruhe capture cross-section data [8] were analyzed with the multilevel R -matrix code FANAC between 10 and 230 keV. Fröhner remarks that above 160 keV the resolution was insufficient for a reliable interpretation of multiplets.

Between 10 and 235 keV, we report 14 well-defined s -wave resonances. (The resonance at 176.16 keV is not clear in transmission, and its s -wave assignment is uncertain.) In the same energy interval, Fröhner reports 10 s -wave resonances (Table III). Because of our higher resolution, we identify only 4 of their 10 s -wave resonances as singlets (at 15.4, 63.0, 136.8, and 159.5 keV) for which the radiation widths can be compared with ours. For the resonance at 63 keV, the discrepancy between the two Γ_γ 's is slightly larger than the combined uncertainties; for the three other resonances, the agreement is good. The other

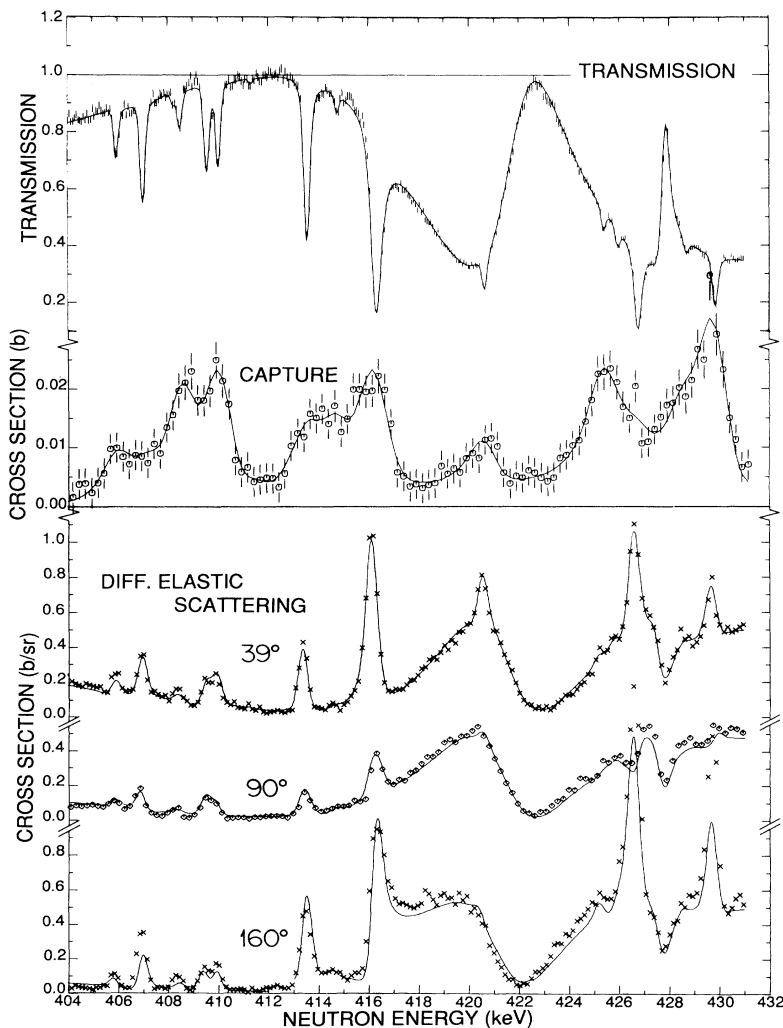


FIG. 7. Top: Concurrent fits, from 404 to 432 keV, to the 200-m transmission data taken with the NE-110 detector and to the capture data obtained with the thick ^{58}Ni sample. Bottom: The data for three of the six differential elastic-scattering angles are compared with the theoretical cross sections calculated with the parameters of Table II.

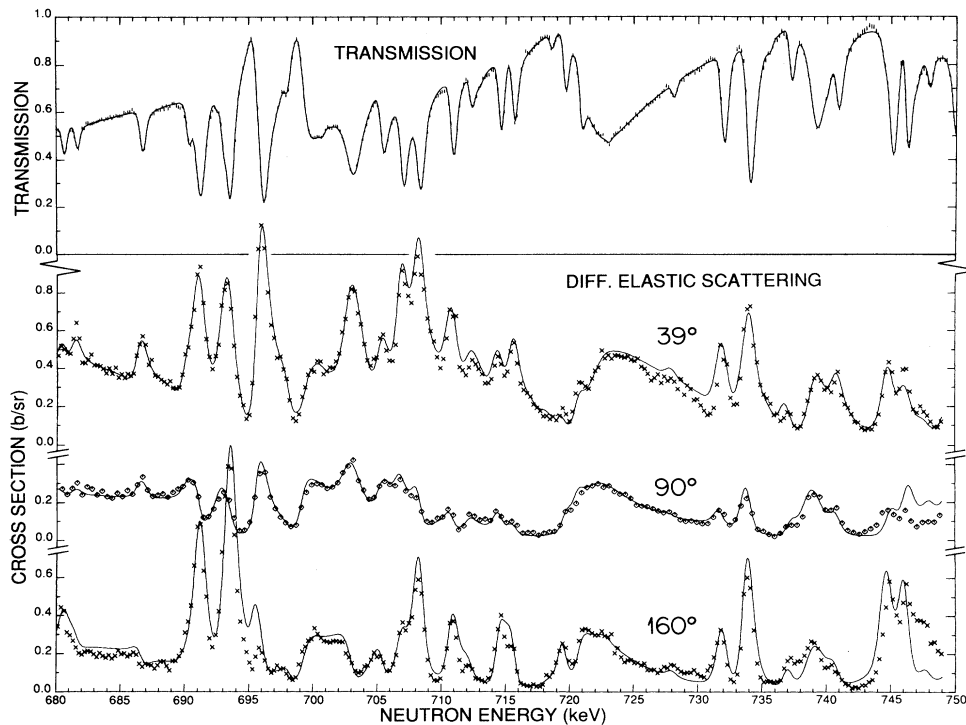


FIG. 8. Fit to the 200-m transmission data from 690 to 750 keV taken with the NE-110 detector. Below, the differential elastic-scattering data is compared to the theoretical calculations for three of the six scattering angles.

6 s -wave resonances are unresolved multiplets of $l=0$ and $l>0$ resonances. It should be noted that above 150 keV the uncertainties on the energies of the s -wave resonances reported by Fröhner are between 2 and 3 keV.

In the 13–120-keV energy region, we analyzed 46 $l>0$ resonances in our capture data, whereas Fröhner reports 36 resonances. Resonance-by-resonance comparison up to 120 keV is given in Ref. [3]. The sums of the capture kernels for the multiplets below 30 keV are compared in Table IV. Five of our weak resonances were not seen in the Karlsruhe data, and five resonances reported by Fröhner as singlets are clearly identified as doublets in our data. Above 120 keV, resonance-by-resonance comparison is no longer possible because of the low-energy resolution of the Karlsruhe experiment: Between 120 and 230 keV, Fröhner reports 12 $l>0$ resonances, while, in the same energy interval, we analyzed 58 $l>0$ resonances.

C. Comparison with the capture kernels of Wisshak *et al.* below 30 keV

Measurements of capture yield in the low-energy region were made by Wisshak *et al.* [9] using Moxon-Rae detectors and various sample thicknesses. The reported values of the parameters for the first s -wave resonance are $E_0=15.35$ keV and $\Gamma_\gamma=1.53\pm 0.10$ eV. This radiation width is in good agreement with Fröhner's value, but 50% larger than ours. The large (31%) uncertainty in our value for Γ_γ at this resonance is due primarily to uncertainty in the scattered neutron correction. If part of that correction were attributed to gamma rays in the

ORELA beam scattered into the detectors by the sample, the 50% discrepancy with Wisshak *et al.* [9] would be reduced.

In the same publication, the capture kernels for three groups of unresolved $l>0$ resonances below 30 keV are also reported. These parameters are compared with ours and those of Fröhner in Table IV. For the first group around 13.5 keV, our value is 11% higher than the value of Wisshak *et al.*, but, as discussed in Sec. III B, a 10% under- or overestimation was possible in the calculation of the capture kernels for this group of narrow resonances because of the proximity of the large s -wave resonance at 15.31 keV. Our parameters are slightly lower (3%) than those of Wisshak *et al.* for the two other groups. Fröhner's parameters are systematically smaller than ours and those of Wisshak *et al.* by as much as 30% for the group around 26 keV.

D. Comparison with ENDF/B-VI evaluation

The resonance parameters given in the ENDF/B-VI evaluation [4] differ only slightly from those reported in this article, since the present analysis is a refinement of the one that yielded the ENDF/B-VI resonance parameters. All experimental and analytical considerations in this paper also applied to the analysis from which the ENDF/B-VI resonance parameters were obtained; the only exception is that a normalization of the transmission data of up to 4% was subsequently interpreted as a water contamination in the sample as reported in Sec. III A. Differences in the capture kernels of the resonances obtained with the parameters in ENDF/B-VI and those re-

TABLE III. Parameters for *s*-wave resonances compared with results of two previous analyses.

E_0 (keV)	Present work		Syme and Bowen [7]		Fröhner [8]	
	Γ_n (eV)	Γ_γ (eV)	E_0 (keV)	Γ_n (eV)	E_0 (keV)	Γ_γ (eV)
15.307	1330±3	0.97±0.30	15.20	1330±120	15.4	1.46±0.22
36.136	18.3±0.3	1.72±0.02	36.102	17±5		
63.337	3798±7	3.5±0.7	63.10	3620±59	63.0	2.3±0.3
83.391	4.0±1.2	1.16±0.11				
108.360	1087±4	4.8±0.3	108.16	1007±24	107.7	3.8±0.8
124.020	459.3±2.8	1.56±0.15	123.804	417±13	124.0	3.5±0.6
137.63	2033±8	2.9±0.8	137.40	2095±43	136.8	2.2±0.4
140.31	3091±10	0.9±0.6	140.08	3048±67	139.7	2.2±0.5
158.13	5246±13	3.3±0.8	157.66	4660±86	159.5	3.0±1.0
168.964	420±4	1.3±0.2	168.66	300±16		
			172.00	10±40		
176.16 ^a	5.0	0.57				
191.913	2479±8	3.3±0.5	191.54	2050±47	193.0	3.0±1.0
206.61	7438±17	6.9±1.0	205.93	5940±110	207.8	4.5±2.0
211.043	60.7±1.7	0.76±0.06	211.00	15±14		
233.06	5654±13	5.3±0.7	232.75	5820±240	230.4	9±4
242.36 ^a	2.6	0.80				
245.553	237.6±2.7	0.55	245.02	143±15		
261.93	15.2±0.9	1.05±0.09				
272.52	5449±13	5.4±0.6	272.07	4990±110		
281.605	1986±8	1.75±0.40	281.06	1610±60		
285.38 ^a	3.5	1.0				
305.405	666±5	2.8±0.5	304.63	547±31		
326.021	1597±7	0.4	325.29	1580±56		
335.19	141.8±2.9	2.54±0.13				
349.660	1778±8	0.8±0.5	349.05	1584±62		
367.737	129.6±2.2	0.4	366.97	84±2		
395.030	693±5	0.5	394.13	600±43		
417.56	9297±29	2.6±1.4	417.20	9930±530		
424.68	7920±29	3.3±1.8	423.98	9090±360		
428.058	1152±15	0.9±0.6	427.175	1590±260		
455.50	1866±12		454.43	1560±110		
462.258	458±5		461.17	310±40		
470.414	489±7		469.40	515±48		
			473.96	155±29		
491.816	182±5					
496.32	1415±10		495.24	1280±70		
507.780	1551±10		506.65	1340±75		
523.54	1294±9		522.26	1160±70		
529.25	203.2±3.7		527.80	300±40		
541.213	519±7		539.89	690±50		
553.73	2409±15		552.27	2770±150		
559.733	852±14		558.17	1260±110		
567.82	9282±34		566.24	7730±260		
588.85	2315±14		587.51	2400±140		
600.69	8070±30		599.27	6570±430		
618.20	404±6		616.50	333±64		
630.96	150±9					
636.42	9340±44		636.18	7460±310		

^a*s*-wave assignment is uncertain.

TABLE IV. Comparison of the sums of the capture kernels of multiplets below 30 keV.

E (keV)	This work ^a	$g\Gamma_n\Gamma_\gamma/\Gamma$ (eV)	
		Fröhner [8] ^b	Wisshak <i>et al.</i> [9]
13.32	0.72 ± 0.07	0.50 ± 0.08	
13.64	0.68 ± 0.07	0.63 ± 0.20	
	1.40 ± 0.14	1.13 ± 0.22	1.26 ± 0.08
19.01	0.077 ± 0.005	0.08 ± 0.02	
20.02	0.29 ± 0.02	0.24 ± 0.05	
21.14	0.76 ± 0.03	0.61 ± 0.10	
	1.13 ± 0.05	0.93 ± 0.11	1.17 ± 0.08
24.76	0.018 ± 0.002		
26.07	0.35 ± 0.02	0.27 ± 0.05	
26.64	0.96 ± 0.04	0.78 ± 0.15	
27.63	0.036 ± 0.004		
	1.36 ± 0.06	1.05 ± 0.16	1.40 ± 0.09

^aA 10% systematic uncertainty was combined with the statistical uncertainty for the first two resonances and a 4% systematic uncertainty for the remaining resonances.

^bUncertainties were assumed to be statistical only.

ported here are much smaller than the experimental uncertainties; for 20% of the resonances, these differences are less than 1%. For average scattering cross sections, the differences are even smaller.

VI. DISCUSSION AND EXTRACTION OF AVERAGE PARAMETERS

A. Reduced neutron width distribution of s -wave resonances

Sixty-one s -wave resonances are reported from 10 to 813 keV. Five of those are weak resonances for which the s -wave assignment is uncertain. The distribution of the normalized reduced neutron widths of these 61 s -wave resonances is represented by the histogram in Fig. 9. Such data are usually assumed to follow a Porter-Thomas distribution [35].

The reduced neutron width at 1 eV for a s -wave resonance is given by

$$\Gamma_n^0 = \Gamma_n [(1 \text{ eV})/E_n]^{1/2},$$

where E_n is the neutron energy in eV.

The Porter-Thomas density function is

$$P(x) = 2(\pi x)^{-1/2} e^{-x/2},$$

where $x = \Gamma_n^0 / \langle \Gamma_n^0 \rangle$ and $\langle \Gamma_n^0 \rangle$ is the average reduced neutron width.

The smooth curve in Fig. 9 is the Porter-Thomas density function normalized to give 47 levels under the curve above 0.1, equal to the observed number of levels above that value of $\Gamma_n^0 / \langle \Gamma_n^0 \rangle$, where we assume that no s -wave resonance was missed. The total number of levels under the Porter-Thomas distribution curve when such a normalization factor is used is 63.7 levels. Since only 61 resonances have an s -wave assignment, we conclude that up to three narrow s -wave resonances could have been missed.

The average reduced neutron width $\langle \Gamma_n^0 \rangle$ is equal to

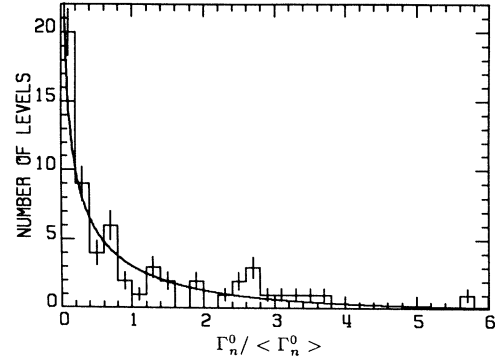


FIG. 9. Distribution of normalized reduced neutron widths for the 61 assigned s -wave resonances in Table II. The smooth curve is the Porter-Thomas distribution normalized to the area under the histogram corresponding to values of $\Gamma_n^0 / \langle \Gamma_n^0 \rangle$ larger than 0.1.

4.3 eV with an uncertainty of 0.7 eV due to the finite sample of 61 levels.

B. s -wave level spacing

The average level spacing D_0 for the s -wave resonances obtained from the 61 s -wave resonances reported in Table II is 13.1 keV with an uncertainty of 0.9 keV due to the finite sample of 60 spacings. In Table V our estimated average level spacing is compared with values obtained from the Syme-Bowen transmission data analysis [7] and from the BNL evaluation of neutron resonance parameters by Mughabghab, Divadeenam, and Holden [29]. Syme and Bowen as well as Mughabghab, Divadeenam, and Holden assumed that some weak s -wave resonances were missed; their reported values of D_0 reflect corrections they made for these missing levels.

The normalized distribution of the s -wave nearest neighbor spacings is compared to the Wigner distribution [36] in Fig. 10. The Wigner density function is expressed as

$$P(x) = \frac{1}{2} \pi x e^{-\pi x^2/4},$$

where $x = d_0 / D_0$ and d_0 is the spacing between neighboring s -wave levels. The Wigner distribution was normalized to the area under the histogram.

The normalized distribution of the s -wave level spacings shown by the histogram in Fig. 10 is in good agreement with the Wigner distribution as confirmed by the values of their second moments. The average value of

TABLE V. Statistical resonance parameters for s -wave resonances.

Source	Energy range (keV)	S_0 (10^4)	D_0 (keV)
Present work	0.1–813	3.2 ± 0.6	13.1 ± 0.9
Syme and Bowen [7]	10–640	2.9 ± 0.6	14.6 ± 0.4
Mughabghab, Divadeenam, and Holden [29]	5–650	2.8 ± 0.6	13.7 ± 2.0

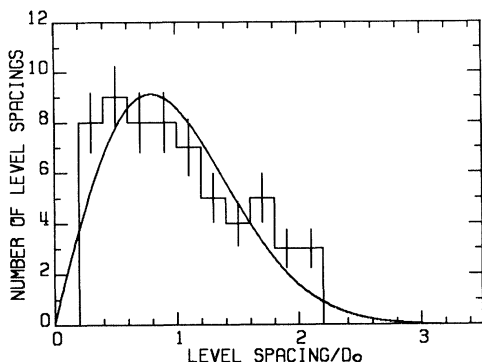


FIG. 10. Distribution of nearest level spacings for the 61 assigned s -wave resonances. The smooth curve is the Wigner distribution normalized to the area under the histogram.

$(d_0/D_0)^2$ for the observed resonances was found to be equal to 1.29 ± 0.16 , which is consistent with the value of 1.27 for a Wigner distribution.

C. Level densities

The results of our transmission and differential elastic-scattering data analysis are compared with the prediction of the Gilbert-Cameron level density model [37].

Gilbert and Cameron started from a Fermi-gas model of the nucleus which was modified to take into account the pairing energy and possible shell model effects, using an effective excitation energy U instead of the actual excitation energy E . The density of levels of total angular momentum J at an excitation energy U is given by

$$\rho(U, J) = \frac{\exp[2\sqrt{aU}]}{12a^{1/4}U^{5/4}} \frac{2J+1}{2\sqrt{2}} \frac{\exp[-(J+\frac{1}{2})^2/2\sigma^2]}{\sigma^3},$$

where a is the Fermi-gas constant and σ^2 is the spin cutoff parameter. The effective excitation energy U is related to the actual excitation energy E above the ground state by the relation $U = E - \Delta$, where Δ is a pairing correction inferred from odd-even mass differences.

In the Fermi-gas model, the spin cutoff parameter is given by

$$\sigma^2 \approx q^2 A^{2/3} \sqrt{aU},$$

where q^2 is related to the mean square of the projection of the total angular momentum of the states around the Fermi level. The value of 0.0888 used for q^2 in this case corresponds to the compound system having a moment of inertia equal to approximately 75% of its rigid moment of inertia [38].

Calculations were made for the s -wave level density using the 61 s -wave resonances reported in Table II between 1 and 813 keV with an uncertainty of three levels, together with the low-lying bound levels of ^{59}Ni taken from the Nuclear Data Sheets [39]. Above the pairing energy gap in ^{59}Ni , the highest level density is observed from 3.46 to 4.2 MeV, where there are 24 levels. This region was therefore selected, and an uncertainty of four levels was used.

The values of the Fermi-gas constant a and the energy shift parameter Δ were obtained using the computer code LEVDEN [40]. This fitting code solves Bayes's equation, using as prior values $5 \pm 10 \text{ MeV}^{-1}$ for the Fermi-gas constant and $0 \pm 3 \text{ MeV}$ for the energy shift parameter. The code was required to produce 24 ± 4 levels in the excitation energy interval of 3.46–4.2 MeV above the ground state of ^{59}Ni and 61 ± 3 s -wave levels in the energy interval of 1–813 keV above the neutron binding energy of 9.000 MeV in ^{59}Ni . The posterior values for the Fermi-gas constant and the energy shift parameter, with their standard deviations, were found to be

$$a = 5.6 \pm 0.2 \text{ MeV}^{-1},$$

$$\Delta = -0.06 \pm 0.39 \text{ MeV},$$

with a correlation coefficient of 0.98. The integral of the theoretical level density formula from 1 to 813 keV for $l=0$ resonances calculated with the above parameter values and their uncertainties is shown by the dashed line on the bottom part of Fig. 11 and is compared with the cumulative sum of the observed s -wave resonances.

Of the 416 $l > 0$ resonances reported in Table II, 74% have a definite l assignment. Therefore we cannot compare separately the level densities for the $l=1$ and 2 resonances with the predictions of the Gilbert-Cameron model. However, assuming that only $l=1$ and 2 resonances were observed in the experiment, we can compare the $l > 0$ level density with the prediction for the sum of the $l=1$ and 2 levels using the a and Δ parameters determined above. Such a comparison is shown on the top part of Fig. 11. As was the case for ^{56}Fe and ^{60}Ni [5,41], the number of $l=1$ and 2 resonances observed above 150

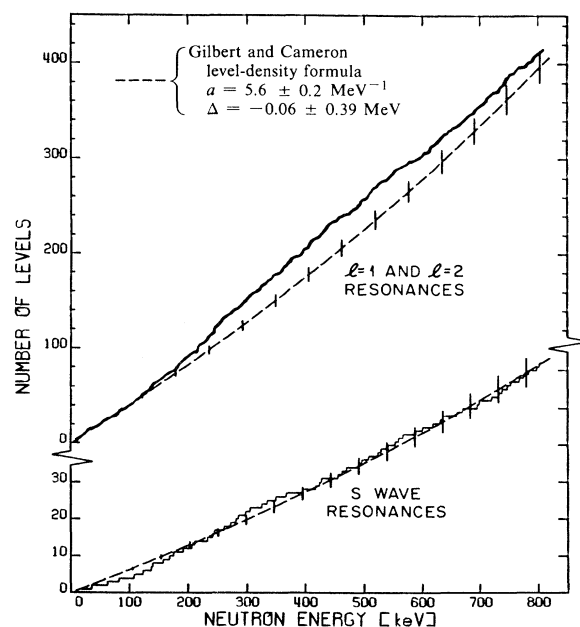


FIG. 11. Cumulative number of resonances for $l=0$ and $l > 0$ as a function of incident neutron energy. The solid lines represent the number of observed resonances; the dashed lines are fits to the data using the Fermi-gas model.

keV is higher than predicted. It is possible that some of the $l=1$ and 2 resonances assigned in the analysis may be $l>2$ resonances. The good agreement with the Gilbert-Cameron formula below 150 keV would then indicate that very few $l=1$ and 2 resonances were missed between 1 and 150 keV.

D. Strength function

For a given angular momentum l , the strength function S_l is defined as

$$S_l = \frac{\langle g\Gamma_n^l \rangle}{(2l+1)D_l},$$

where $\langle g\Gamma_n^l \rangle$ is the average of the reduced widths times their statistical weight factors g and D_l is the average level spacing. For the $l=0$ resonances, S_0 is the slope of the plot of the cumulative sum of the reduced widths as a function of the incident neutron energy.

Such a plot for the 61 assigned s -wave resonances is given in Fig. 12. In this case the staircase plot is well approximated by a straight line over the complete analyzed energy range. The s -wave strength function is equal to $(3.2 \pm 0.6) \times 10^{-4}$ and is compared in Table V to the value obtained by Syme and Bowen [7] from their transmission data analysis below 640 keV. The recommended value from the evaluation of Mughabghab, Divadeenam, and Holden [29] is $(2.8 \pm 0.6) \times 10^{-4}$.

Since the differential elastic-scattering data allowed us to assign a definite orbital angular momentum to most of the large non- s -wave resonances, it is meaningful to determine the p - and d -wave strength functions for those large resonances. Even though these resonances represent only about 64% of the total number of the $l>0$ resonances, they contribute most of the strength.

For the 124 resonances having a definite p -wave assignment, the cumulative plot of the reduced neutron widths, times g , is well represented by a linear function of neutron energy, as shown in Fig. 13. The value of the strength function S_1 over the complete energy range is one-third of the slope of the straight line, yielding $S_1 = (0.65 \pm 0.09) \times 10^{-4}$, which is slightly larger than the value of $(0.5 \pm 0.1) \times 10^{-4}$ reported in Ref. [29].

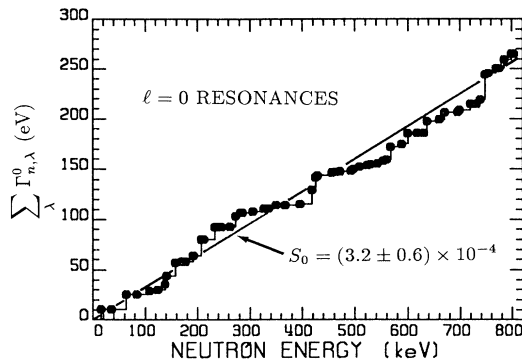


FIG. 12. Sum of the reduced neutron widths for s -wave resonances as a function of incident neutron energy. The strength function S_0 is given by the slope of the straight line.

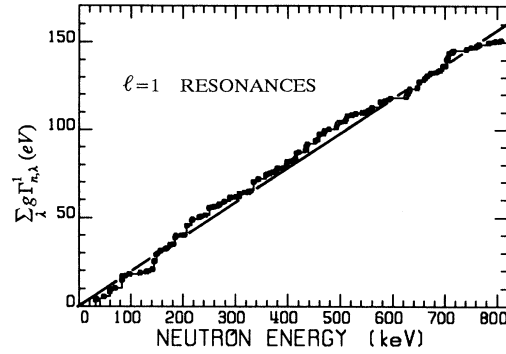


FIG. 13. Weighted sum of reduced neutron widths for $l=1$ resonances as a function of incident neutron energy. Only resonances with definite l assignment were used to generate the histogram.

Figure 14 shows the sum of the reduced neutron widths times g as a function of incident energy for the 141 d -wave resonances having a definite l assignment. It can be represented by a straight line only up to ≈ 350 keV. It is not clear how to interpret the observed features above that energy, especially the large step around 600 keV. The average strength function S_2 over the analyzed energy range is one-fifth of the slope of the straight line shown on Fig. 14, yielding $S_2 = (1.4 \pm 0.2) \times 10^{-4}$.

E. Average radiation widths

Of the 30 s -wave resonances reported between 1 and 450 keV, three are weak resonances in the transmission data. Their s -wave assignments are uncertain; therefore, they were not used in the computation of the s -wave resonance average radiation width.

The mean value of the distribution of the radiation widths of the remaining 27 s -wave resonances is equal to 2.3 eV, and the standard deviation of the distribution is 1.7 eV. As indicated by note 3 in Table II, 19 of these 27 s -wave resonances had their radiation widths corrected for the neutron sensitivity of the detector. This mean value is consistent with the previous ^{58}Ni capture mea-

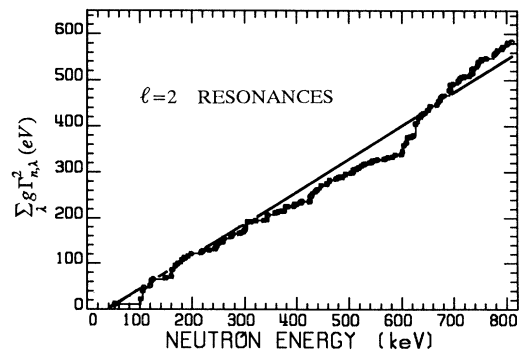


FIG. 14. Weighted sum of reduced neutron widths for $l=2$ resonances as a function of incident neutron energy. Only resonances with definite l assignment were used to generate the histogram.

surement of Ernst, Fröhner, and Kompe [34], which yields a value of $\langle \Gamma_\gamma \rangle$ of 2.6 ± 0.9 eV based on 5 *s*-wave resonances below 160 keV.

For the $l > 0$ resonances, only the resonances whose angular momentum and spin could be determined through the analysis of the differential elastic-scattering data were used in the computation of the average radiation widths. Of these resonances we eliminated those which were part of a multiplet, since for multiplets the sum of the capture areas is well determined, but the capture area of each individual resonance is not.

The mean value of the distribution of the radiation widths of the *p*-wave resonances, calculated from the parameters of 39 resonances, is equal to 0.77 eV, and the standard deviation is 0.32 eV.

For the *d*-wave resonances, the mean value of the distribution of the radiation widths calculated from the parameters of only 9 resonances is equal to 1.4 eV and the standard deviation is 0.5 eV. The mean value of the distribution would be 1.2 eV if the calculation included the 37 resonances for which the $l=2$ assignment is determined but the spin assignment is not. The fact that this value of 1.2 eV is close to the one obtained with the 9 single resonances for which the spin and parity are known indicates that the spins we assigned to these 37 resonances based solely on the value of $g\Gamma_\gamma$ are consistent with the little information we have for the *d*-wave resonances.

F. Average capture cross section

The average capture cross sections given in Table VI in lethargy intervals up to 450 keV were obtained by summing the capture areas of the resonances in each interval, including the contributions from the negative-energy resonances. The uncertainties include the statistical uncertainties as well as the uncertainties from the correction for the detector's neutron sensitivity. The uncertainties in the correction for the detector neutron sensitivity were treated as uncorrelated. Uncertainties due to problems with the weighting function (see Sec. II B) are assumed to place a lower limit of 15% on the value of the uncertainty for the average capture cross section.

The average capture cross section above 450 keV was obtained from the average capture data in the following manner: From 450 to 1400 keV, the thick sample data were corrected for sample thickness effects, primarily capture after scattering, using strength functions and averaging over a Porter-Thomas distribution in each energy interval. Average scattering cross sections were computed from the present work up to 800 keV and from the literature up to 1000 keV and then extrapolated to 1400 keV. Inelastic scattering to the first 2^+ level begins at a threshold of 1480 keV; the detectors responded strongly to the inelastic gamma ray. These sample thickness corrections ranged from 10% to 3% in the 450–1400-keV energy range for the intervals shown.

The average capture cross section obtained from this analysis is shown from 1 keV to 1 MeV by the histogram in Fig. 15. The smooth line is the result of the theoretical calculation provided by P. G. Young of Los Alamos Na-

tional Laboratory from the reaction theory code COMNUC [42]. Width fluctuation corrections were made using Moldauer's integral method [43] and an approximation from Tepel, Hofmann, and Weidenmüller [44] for the number of degrees of freedom. COMNUC calculates the capture cross section by using transmission coefficients for gamma rays derived from the width of the *E1* giant dipole resonance [45]. Only *E1* transitions were considered, and the gamma-ray partial widths are functions only of the gamma-ray energy E_γ , the initial level spin, and the final level spin. Level densities and their spin distributions were obtained from the Gilbert-Cameron formula [37]. The parameters of the giant dipole resonance were taken from Ref. [46]. In the case of ^{58}Ni , the giant dipole resonance is double humped with one resonance at 16.3 MeV which is 2.44 MeV wide and the other at 18.51 MeV which is 6.37 MeV wide, the ratio of the peak cross section for the second resonance to the first resonance being 1.6. The absolute magnitude of the giant dipole resonance was adjusted to yield the experimentally observed value of $2\pi\langle \Gamma_{\gamma_0} \rangle / D_0$. This model usually predicts the

TABLE VI. Average capture cross section.

Energy range (keV)	Average capture cross section (mb)	
	This analysis ^a	Fröhner [8]
1.00–1.26	18.6±2.8	
1.26–1.59	16.0±2.4	
1.59–2.00	13.6±2.0	
2.00–2.51	11.6±1.7	
2.51–3.16	9.7±1.5	
3.16–3.98	8.1±1.2	
3.98–5.01	6.7±1.0	
5.01–6.31	5.6±0.8	
6.31–7.94	5.1±0.8	2.6±0.3
7.94–10.00	4.7±0.7	3.3±0.5
10.00–12.59	6.8±1.4	6.6±1.0
12.59–15.85	194±29	195±25
15.85–20.0	14.8±4.1	26.3±3.2
20.0–25.1	44.2±6.6	35.2±4.4
25.1–31.6	34.1±5.1	26.2±3.9
31.6–39.8	75.9±11.4	55.7±5.0
39.8–50.1	12.9±1.9	10.6±1.3
50.1–63.1	39.1±5.9	31.4±2.3
63.1–79.4	11.0±1.7	9.8±0.7
79.4–100.0	24.8±3.7	17.3±1.7
100.0–125.9	34.7±5.2	22.0±2.1
125.9–158.5	21.0±3.2	12.6±1.0
158.5–199.5	23.4±3.5	16.5±2.4
199.5–251.2	19.2±2.9	13.1±3.3
251.2–316.2	15.3±2.3	
316.2–398.1	12.7±1.9	
398.1–450	13.0±2.0	
450–500	12.8±1.9	
500–600	12.0±1.8	
600–800	12.2±1.8	
800–1000	11.4±1.7	
1000–1200	12.3±1.8	
1200–1400	14.1±2.1	

^aThe average capture cross section above 450 keV was obtained from the capture data.

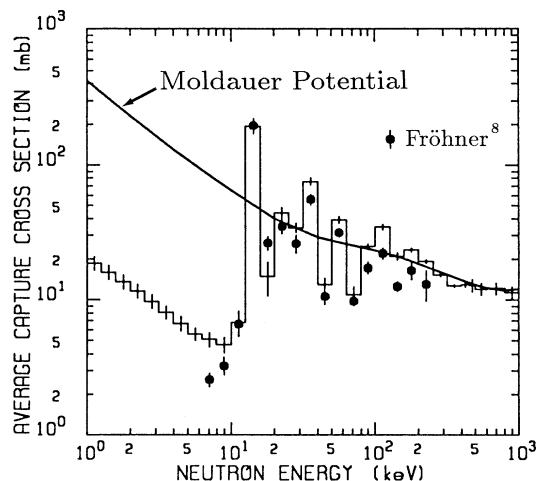


FIG. 15. Average capture cross section from 1 keV to 1 MeV as a function of incident neutron energy. The smooth curve is given by the tail of the double-humped giant dipole $E1$ normalized by 0.65. The dots represent the average capture cross section from Fröhner's evaluation.

capture cross sections within a factor of 2. In this case the capture cross section was overpredicted, and the theoretical predictions in Fig. 15 were normalized by a factor of 0.65.

The dots in Fig. 15 correspond to the average capture cross section obtained from the parameters of Fröhner [8], which are given in Table VI. Fröhner's data give systematically smaller values than those obtained from our data.

The average capture cross section calculated with the parameters given in the ENDF/B-VI evaluation between 1 and 450 keV is identical to the value reported in this

work since the parameters were obtained from the same ORELA capture data analysis.

G. Stellar average cross section

The stellar, or Maxwellian, averaged capture cross sections shown in Table VII were obtained from the stellar reaction rate formula

$$\langle \sigma(E)E^{1/2} \rangle_{kT} = \int_0^{\infty} \sigma_{\text{capture}} E^{1/2} W(E, kT) dE,$$

where $W(E, kT)$ is the Maxwellian weighting factor,

$$W(E, kT) = \frac{2}{\sqrt{\pi}} (kT)^{-2} e^{-E/kT},$$

and the capture cross section σ_{capture} is generated from the resonance parameters. The integrations were performed numerically using the code SAMMY [26]; values virtually identical to these were obtained by Winters [47] of Denison University, using the numerical method of Beer, Voss, and Winters [48] with the resonance parameters found in this study.

Uncertainties on the stellar average cross sections quoted in Table VII are estimated at 15%, primarily due to problems with the weighting function as described at the end of Sec. II B.

The present results range from 3% to 12% lower than those given in the compilation of Beer, Voss, and Winters [48].

Earlier estimates for the Maxwellian-averaged capture cross section appearing in the literature include the following: Allen, Gibbons, and Macklin [49] reported a value of 17 ± 3 mb at $kT = 30$ keV based on a measurement [50] of the capture cross section. Wisshak *et al.* [9] reported a value of 39.0 ± 2.5 mb based on a measurement of the radiation width of the 15.3-keV resonance using a

TABLE VII. Maxwellian-averaged capture cross sections (mb).

kT (keV)	This work	Others
5.0	39.8	
6.0	45.0	
7.0	48.4	
8.0	50.5	
9.0	51.6	
10.0	52.0	
12.5	51.5	
15.0	49.9	
17.5	48.0	
20.0	46.2	
25.0	42.9	39.0 ± 2.5
30.0	40.2	17 ± 3 27.4 29
35.0	38.1	(Wisshak <i>et al.</i> [9], experiment)
40.0	36.3	(Allen, Gibbons, and Macklin [49], experiment)
45.0	34.8	(Harris [51], theory)
50.0	33.5	(Woosley <i>et al.</i> [52], theory)
60.0	31.3	
70.0	29.5	
85.0	27.2	
100.0	25.3	

neutron spectrum approximating a Maxwellian distribution with $kT=25$ keV. Harris [51] and Woosley *et al.* [52] provided theoretical estimates of 27.4 and 29 mb, respectively, at $kT=30$ keV. Our results agree more closely with those of Wisshak *et al.* than with those of Allen, Gibbons, and Macklin. Our results also show strong peaking near 10 keV, reflecting the influence of the large s -wave resonance at 15.3 keV; the theoretical estimates of Harris and Woosley *et al.* may not have included this large resonance.

VII. CONCLUSIONS

The results of this analysis considerably improve upon our knowledge of resonances observed in the interaction of neutrons with ^{58}Ni . Prior to this work, 142 resonances had been reported below 650 keV, whereas we were able to observe 317 resonances in our transmission and capture data up to that energy, plus 61 resonances which were too weak to be seen in the transmission data but which were clearly observed and analyzed in the capture data. This analysis also covers a wider range of energies than previously reported; our new set of resonance parameters provides a complete and accurate description of the scattering cross section from thermal to 813 keV.

The differential cross-section data allowed us to make a definite l assignment for 75% of the $l > 0$ resonances analyzed in the transmission data above 30 keV (265 resonances out of 354). A definite J assignment could be made for 146 of these 265 $l > 0$ resonances. Since only 24 $l > 0$ resonances have a width comparable to or larger than the resolution of the transmission measurements, very few spin assignments could have been made if the differential cross-section data had not been measured.

The reduced neutron width distribution of the 61 s -wave resonances reported in this analysis is in good agreement with the Porter-Thomas distribution even though it seems to indicate that three narrow s -wave resonances could have been missed. The distribution of the nearest neighbor spacing is in good agreement with the Wigner distribution.

From the cumulative sum of the reduced neutron

widths times the statistical weight factor, the strength functions for the s -, p -, and d -wave resonances were deduced even though the plot of the sum of the reduced neutron widths for the d -wave resonances is reasonably linear only for levels below 400 keV. The cumulative number of $l=0$ and $l > 0$ resonances was compared with the prediction of the Fermi-gas level density model, which underpredicts the number of observed $l > 0$ resonances.

Of the resonances analyzed in the three kinds of data below 450 keV, those which could have their angular momentum definitely assigned were used to compute the average radiation width for each l value. The average capture cross section was calculated in lethargy intervals up to 450 keV using all the resonances analyzed in the capture data. Above 450 keV and up to 1400 keV, the corrected capture data were used.

The results reported in this paper could be significantly improved with higher resolution in the capture data, with a correct weighting function for high-energy gamma rays, and with a more accurate treatment of the multiple scattering in the capture data analysis.

The extension of our knowledge of the resonances to higher energy is of significant importance in reactor calculations since it eliminates the need to deal with a very approximate unresolved resonance formalism.

ACKNOWLEDGMENTS

The authors are grateful to P. G. Young of Los Alamos National Laboratory for performing the average capture cross-section calculations. We are also indebted to Professor R. R. Winters of Denison University, Granville, Ohio, for valuable discussions and preliminary calculations of the stellar averages. The authors also wish to acknowledge T. A. Lewis and the ORELA operators for efficient and capable accelerator operation. This research was sponsored by the Office of Energy Research, Division of Nuclear Physics, U.S. Department of Energy, under Contract No. DE-AC05-84OR21400 with Martin Marietta Energy Systems, Inc.

-
- [1] F. G. Perey, G. T. Chapman, W. E. Kinney, and C. M. Perey, in *Neutron Data of Structural Materials for Fast Reactors, Geel, 1977*, edited by K. H. Böckhoff (Pergamon, New York, 1979), p. 530.
- [2] C. M. Perey, F. G. Perey, J. A. Harvey, N. W. Hill, and R. L. Macklin, in *Nuclear Data for Basic and Applied Science, Santa Fe, 1985*, edited by P. G. Young *et al.* (Gordon and Breach, New York, 1986), Vol. 2, p. 1639.
- [3] C. M. Perey, F. G. Perey, J. A. Harvey, N. W. Hill, N. M. Larson, and R. L. Macklin, Oak Ridge National Laboratory Report No. ORNL/TM-10841, 1988.
- [4] *ENDF/B-IV Summary Documentation*, edited by P. F. Rose, National Nuclear Data Center Report No. BNL-NCS-17541 (ENDF-201, 4th Edition, 1991).
- [5] C. M. Perey, F. G. Perey, J. A. Harvey, N. W. Hill, and N. M. Larson, Oak Ridge National Laboratory Report No. ORNL/TM-11742, 1990.
- [6] D. B. Syme, P. H. Bowen, and A. D. Gadd, in [1], p. 703.
- [7] D. B. Syme and P. H. Bowen, *Neutron Physics and Nuclear Data for Reactors, Harwell, 1978* (OECD, Paris, 1978), p. 319.
- [8] F. Fröhner, in [1], p. 138.
- [9] K. Wisshak, F. Käppeler, G. Reffo, and F. Fabbri, *Nucl. Sci. Eng.* **86**, 168 (1984).
- [10] R. L. Macklin, D. M. Drake, and E. D. Arthur, *Nucl. Sci. Eng.* **84**, 98 (1983).
- [11] R. L. Macklin, N. W. Hill, and B. J. Allen, *Nucl. Instrum. Methods* **96**, 509 (1971).
- [12] R. L. Macklin and B. J. Allen, *Nucl. Instrum. Methods* **91**, 565 (1971).

- [13] R. L. Macklin, J. Halperin, and R. R. Winters, *Nucl. Instrum. Methods* **164**, 213 (1979).
- [14] C. Le Rigoleur (private communication).
- [15] R. L. Macklin, *Nucl. Sci. Eng.* **95**, 200 (1987).
- [16] D. B. Gayther, J. E. Jolly, and R. B. Thom, in *Proceedings of the International Conference on Nuclear Data for Science and Technology, Mito, Japan, 1988*, edited by S. Igarasi (Saikon, Tokyo, Japan, 1988), p. 157.
- [17] F. G. Perey, J. O. Johnson, T. A. Gabriel, R. L. Macklin, and R. R. Winters, in [16], p. 379.
- [18] M. Sowerby and F. Corvi, in [16], p. 37.
- [19] F. Corvi, G. Fioni, A. Mauri, and K. Athanasopoulos, in *Proceedings of the International Conference on Nuclear Data for Science and Technology, Jülich, 1991*, edited by S. M. Qain (Springer-Verlag, Berlin, Germany, 1992), p. 44.
- [20] R. L. Macklin, *Nucl. Sci. Eng.* **86**, 362 (1984).
- [21] D. J. Horen, C. H. Johnson, J. L. Fowler, A. D. MacKellar, and B. Castel, *Phys. Rev. C* **34**, 429 (1986).
- [22] N. W. Hill, J. A. Harvey, D. J. Horen, G. L. Morgan, and R. R. Winters, *IEEE Trans. Nucl. Sci.* **NS-32**, 367 (1985).
- [23] D. C. Larson, N. M. Larson, J. A. Harvey, F. G. Perey, D. E. Pierce, and R. H. Seals, Oak Ridge National Laboratory Report No. ORNL/TM-9097, 1985.
- [24] D. C. Larson, N. M. Larson, and J. A. Harvey, Oak Ridge National Laboratory Report No. ORNL/TM-8880, 1984.
- [25] C. W. Reich and M. S. Moore, *Phys. Rev.* **111**, 929 (1958).
- [26] N. M. Larson and F. G. Perey, Oak Ridge National Laboratory Report No. ORNL/TM-7485, 1980; Oak Ridge National Laboratory Report No. ORNL/TM-9179, 1984; Report No. ORNL/TM-9179/R1, 1985; Report No. ORNL/TM-9179/R2, 1989.
- [27] C. M. Perey, F. G. Perey, J. A. Harvey, N. W. Hill, and N. M. Larson, in [19], p. 41.
- [28] S. N. Cramer and F. G. Perey, *Nucl. Sci. Eng.* **111**, 102 (1992).
- [29] S. F. Mughabghab, M. Divadeenam, and N. E. Holden, *Neutron Resonance Parameters and Thermal Cross Sections*, Neutron Cross Sections, Vol. 1 (Academic, New York, 1981), p. 28-2.
- [30] R. L. Macklin, *Nucl. Sci. Eng.* **59**, 12 (1976).
- [31] B. J. Allen, A. R. de L. Musgrove, R. L. Macklin, and R. R. Winters, in [1], p. 506.
- [32] F. G. Perey, Oak Ridge National Laboratory Report No. ORNL/TM-1112, 1989.
- [33] J. M. Blatt and L. C. Biedenharn, *Rev. Mod. Phys.* **24**, 258 (1952).
- [34] A. Ernst, F. H. Fröhner, and D. Kompe, *Proceedings of the International Conference on Nuclear Data for Reactors*, Helsinki, 1970 (IAEA, Vienna, 1970), Vol. 1, p. 633.
- [35] C. E. Porter and R. G. Thomas, *Phys. Rev.* **104**, 483 (1956).
- [36] E. P. Wigner, in *Proceedings of the Gatlinburg Conference on Neutron Time-of-Flight Methods*, Oak Ridge National Laboratory Report No. ORNL-2309, 1957, p. 57.
- [37] A. Gilbert and A. G. W. Cameron, *Can. J. Phys.* **43**, 1446 (1965).
- [38] W. Dilg, W. Schantl, H. Vonach, and M. Uhl, *Nucl. Phys.* **A217**, 269 (1973).
- [39] P. Anderson, L. P. Ekstrom, and J. Lyttkens, *Nucl. Data Sheets* **39**, 641 (1983).
- [40] N. M. Larson, D. C. Larson, C. M. Perey, and F. G. Perey, Oak Ridge National Laboratory Report No. ORNL/TM-10843 (in progress).
- [41] C. M. Perey, J. A. Harvey, R. L. Macklin, F. G. Perey, and R. R. Winters, *Phys. Rev. C* **27**, 2556 (1983).
- [42] C. L. Dunford, Report No. AI-AEC-12931, 1970.
- [43] P. A. Moldauer, *Phys. Rev. C* **14**, 764 (1976).
- [44] J. W. Tepel, H. M. Hofmann, and H. A. Weidenmüller, *Phys. Lett.* **49B**, 1 (1974).
- [45] P. Axel, *Phys. Rev.* **126**, 671 (1962).
- [46] B. L. Berman, Report No. UCRL-78482, 1976.
- [47] R. R. Winters (private communication).
- [48] H. Beer, F. Voss, and R. R. Winters, *Astrophys. J. Suppl.* **80**, 403 (1992).
- [49] B. J. Allen, J. H. Gibbons, and R. L. Macklin, *Adv. Nucl. Phys.* **4**, 205 (1971).
- [50] R. W. Hockenbury, Z. M. Bartolome, W. R. Moyer, J. R. Tatarczuk, and R. C. Block, *Phys. Rev.* **178**, 1746 (1969).
- [51] M. J. Harris, *Astrophys. Space Sci.* **77**, 357 (1978).
- [52] S. E. Woosley, W. A. Fowler, J. A. Holmes, and A. B. Zimmerman, *At. Data Nucl. Data Tables* **22**, 371 (1978).